No. 16

Measurement Good Practice Guide

Extensional flow properties of polymer melts using converging flow methods

Martin Rides and Crispin Allen

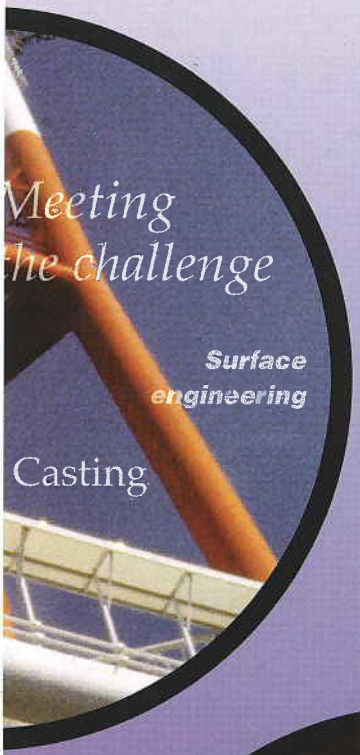

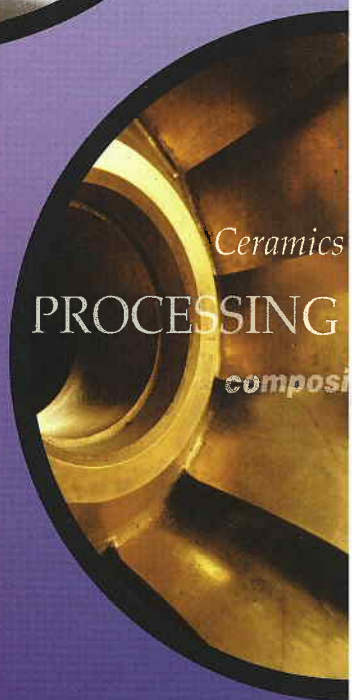

NPL
National Physical Laboratory

The National Physical Laboratory is operated on behalf of the DTI by NPL Management Limited, a wholly owned subsidiary of Serco Group plc

Measurement Good Practice Guide No. 16

Extensional flow properties of polymer melts using converging flow methods

Martin Rides and Crispin Allen
Centre for Materials Measurement and Technology
National Physical Laboratory

Abstract:

In many forming processes the polymer melt undergoes predominantly extensional deformation, for example in blow moulding and film blowing. Furthermore, the extensional flow behaviour of melts differs significantly from their shear flow behaviour. Thus extensional flow measurement methods are necessary to characterise most appropriately the melt behaviour. Such data can be used for the development and selection of materials and for improving processing.

Converging flow methods can be used to assess the extensional flow behaviour of polymer melts. This document provides guidance on the use of converging flow methods for determining the extensional flow behaviour of polymer melts. It defines good practice in using converging flow models and in the generation of data to input into the models. An intercomparison of the predictions of the selected converging flow models and an assessment of the uncertainties in the predictions are presented. Finally, the guide compares the converging flow model predictions for selected materials with data obtained using a tensile testing method to demonstrate the validity of the converging flow approach.

ISSN 1368-6550

March 1999

National Physical Laboratory
Teddington, Middlesex, United Kingdom, TW11 0LW

This guide was produced as part of the *Materials Measurement* programme, a programme of underpinning research supported by the department of trade and Industry and disseminated by the National Physical Laboratory.

For further information on *Materials Measurement* contact the Materials Enquiry Point at the National Physical Laboratory:
Tel: 0181 943 6701
Fax: 0181 943 7160
E-mail: materials@npl.co.uk

Extensional flow properties of polymer melts using converging flow methods

Contents

Tables

Figures

Appendices

Foreword

This guide describes methods for determining the extensional flow behaviour of plastics melts using converging flow models. This guide should be used in conjunction with the ISO standard *ISO 11443:1995 Determination of the fluidity of plastics using capillary and slit-die rheometers* [1] that defines the procedure for capillary extrusion rheometry of plastics. This standard is identical to the British standard *BS2782: Part7: Method 722B: 1996.*

In the drafting of this guide, it has been assumed that the collection and analysis of data will be carried out by suitably qualified and experienced personnel.

Users of this guide are invited to give feedback to the author on any issues related to its use or content.

1 Scope

This guide:

- gives practical advice on how to obtain extensional viscosity values of polymer melts from measurement of the pressure drop in capillary die extrusion tests,
- describes and discusses the converging flow models that are available for interpreting entrance pressure drop data in terms of extensional viscosity,
- defines good practice in the generation of shear viscosity and entrance pressure drop data to input into the models,
- presents an assessment of the effect of errors in the entrance pressure drop and shear viscosity data on the derived extensional viscosity values, and
- intercompares the predictions of the selected converging models and compares predictions with data obtained using a tensile testing method for select materials, thereby demonstrating the validity of the converging flow approach.

2 Introduction

In many plastics forming processes the melt undergoes predominantly extensional deformation, for example in blow moulding, fibre spinning, film blowing and vacuum forming [2-4]. Extensional flow also occurs in profile extrusion and in injection moulding, for example in the nozzle of the injection moulding machine and in passing from the runner to the gate of the moulding. Furthermore, the extensional flow behaviour of polymer melts can differ significantly from their shear flow behaviour. For example, extensional viscosity values may be an order of magnitude or more higher than shear viscosity values and may also exhibit additional trends not normally exhibited in shear, for example strain hardening. Thus extensional flow measurement methods are necessary to characterise most appropriately the melt behaviour. Such data can be used for the development and selection of materials, quality control and for process design and optimisation.

There are two basic approaches to determining extensional flow properties of polymer melts: either using tensile testing methods or converging flow methods (the term "converging" is used herein and is synonymous with "contraction"). Tensile testing methods were reviewed

and reported elsewhere [5]. The converging flow approach for determining the extensional flow behaviour of polymer melts is based on the measurement of the resistance to flow in a contraction geometry, Figure 1. A converging flow is, by definition, a type of extensional flow. It is expected therefore that extensional viscosity might be obtained from the measurement of pressure drop and flow rate in a converging flow. The approach of using converging flow methods is appealing as experimental data are easily obtained from capillary extrusion rheometry testing, normally carried out to determine the shear viscosity of materials. Thus extensional viscosity values can be obtained from the same capillary rheometry tests as already carried out to determine shear viscosity at little or no extra experimental cost.

The converging flow approach can be used to assess the extensional flow behaviour of polymer melts. However, there are several models available that have been developed to interpret the experimental data obtained from capillary extrusion measurements. A critical review of converging flow models for determining the extensional viscoelastic behaviour of polymer melts is presented elsewhere [6]. The review assessed the models, their use and the very limited comparison of data thus obtained with other methods. The review can be used to easily source information on converging flow testing on a range of polymer melts.

The converging flow models due to Cogswell [7], Binding [8,9], and Gibson [10] were selected from that review for consideration herein, along with a further model based on a development of the Cogswell model by Rides - see Appendix A7. The Cogswell model is the most popular of the models, as indicated by usage in the literature [6].

3 Definitions

The definitions 3.1 - 3.3 and 3.5 are given in full the ISO standard on capillary extrusion rheometry of polymer melts (*ISO 11443 : 1995 - Determination of the fluidity of plastics using capillary and slit-die rheometers*, also identical with *BS2782: Part 7: Method 722B: 1996*). Also, for a further detail of definitions related to extensional flows and flow behaviour see Appendix A1.

3.1 Apparent shear rate

Apparent shear rate, $\dot{\gamma}_{ap}$ (s^{-1}): the shear rate that the melt at the wall would experience at the given volume flow rate if its behaviour were Newtonian.

3.2 Shear rate or true shear rate

Shear rate or true shear rate, $\dot{\gamma}$ (s^{-1}): the shear rate obtained from the apparent shear rate $\dot{\gamma}_{ap}$ by taking into account the deviation from Newtonian behaviour (where the term shear rate is used herein it specifies the true shear rate).

3.3 Shear stress or true shear stress

Shear stress or true shear stress, τ (Pa): the shear stress to which the melt in contact with the die wall is subjected.

3.4 Apparent shear viscosity

Apparent shear viscosity, η_{ap} (Pa.s): the ratio $\tau / \dot{\gamma}_{ap}$ of shear stress τ to apparent shear rate $\dot{\gamma}_{ap}$. This differs from the *apparent viscosity* that is defined in ISO11443 in that the *apparent shear viscosity* is corrected for entrance pressure and exit pressure drop effects unlike the *apparent viscosity*.

3.5 Shear viscosity

Shear viscosity, η (Pa.s): the viscosity in steady shear, defined as the ratio $\tau / \dot{\gamma}$ of shear stress τ to shear rate $\dot{\gamma}$.

3.6 Bagley plot

A plot of extrusion pressure versus die length to radius ratio, for constant flow rate and hence constant apparent shear rate data. It is used to determine the shear stress, and hence apparent shear viscosity, and entrance pressure drop values, Figure 2.

3.7 Entrance pressure drop

Entrance pressure drop, P_{ent} (Pa): the value of the intercept of the constant flow rate Bagley plot with the pressure axis, obtained using a Bagley plot.

3.8 Entry angle

Entry angle, α (°): see Figure 1.

3.9 Diameter contraction ratio

The ratio of the barrel diameter to die bore diameter.

3.10 Area contraction ratio

The ratio of the barrel cross sectional area to die bore cross sectional area.

3.11 Elongation ratio

Elongation ratio (ER): the ratio of the current length ℓ to the initial length ℓ_o of the specimen:

$ER = \ell / \ell_o$.

3.12 Hencky strain

Also referred to as the natural or true strain. It is given by the natural logarithm of the elongation ratio:

$\varepsilon = \ln(\ell / \ell_o)$

3.13 Hencky strain rates

Hencky strain rate $\dot{\varepsilon}$ (s^{-1}):

$\dot{\varepsilon} = 1/\ell \times \partial\ell / \partial t$.

3.14 Net tensile stress

The net tensile stress σ_E (Pa): in tensile (simple) extension it is defined by

$\sigma_E = \sigma_{11} - \sigma_{22} = \sigma_{11} - \sigma_{33} = \sigma_{zz} - \sigma_{rr}$

where σ_{ii} is a stress tensor in rectangular of axisymmetric coordinates.

3.15 The tensile stress growth coefficient

The tensile stress growth coefficient η_E^+ (Pa.s): the ratio of the net tensile stress to strain rate

$$\eta_E^+(t, \dot{\varepsilon}) = \sigma_E / \dot{\varepsilon}$$

where t is time, and + indicates start-up of flow.

3.16 Tensile viscosity

The tensile viscosity η_E (Pa.s) is defined by

$$\eta_E(t, \dot{\varepsilon}) = \lim_{t \to \infty} [\eta_E^+(t, \dot{\varepsilon})]$$

It is the limiting tensile stress growth coefficient value and represents an equilibrium extensional viscosity.

3.17 Extensional viscosity

The term extensional viscosity λ (Pa.s) is used to define the equilibrium extensional viscosity derived using converging flow analysis. Equilibrium implies that it is independent of strain and time, but not of strain rate.

4 Symbols

Symbols are defined here where they are not defined above in Section 3. Symbols only used in the Appendices are defined therein.

L - capillary die length, m.
R_i - barrel radius, m.
R_o - capillary die radius, m.
Q - flow rate, m^3s^{-1}.
θ - temperature, °C
η_o - coefficient in the shear viscosity power-law equation, $\eta = \eta_o \dot{\gamma}^{n-1}$, $Pa.s^n$.
n - coefficient in the shear viscosity power-law equation, $\eta = \eta_o \dot{\gamma}^{n-1}$.
λ_o - coefficient in the extensional viscosity power-law equation, $\lambda = \lambda_o \dot{\gamma}^{m-1}$, $Pa.s^m$.

m - coefficient in the extensional viscosity power-law equation, $\lambda = \lambda_o \dot{\gamma}^{m-1}$.

N_1 - first normal stress difference, Pa.

$N_{1,o}$ - coefficient in the first normal stress difference power-law equation, $N1 = N_{1,o}\dot{\gamma}^{p+1}$, $Pa.s^{p+1}$.

p - coefficient in the first normal stress difference power-law equation, $N1 = N_{1,o}\dot{\gamma}^{p+1}$.

$P_{ent,}$ - coefficient in the entrance pressure drop power-law equation, $P_{ent} = P_{ent,o}Q^s$, $Pa.(m^3s^{-1})^{-s}$

s - coefficient in the entrance pressure drop power-law equation, $P_{ent} = P_{ent,o}Q^s$.

5 Converging flow methods

5.1 General considerations

As discussed in Section 2 a critical review of converging flow models for determining the extensional viscoelastic behaviour of polymer melts is presented elsewhere [6]. It assessed the models, their use and the very limited comparison of data thus obtained with other methods. The converging flow models presented in the literature encompass the use of various entry geometries to the die or special testing conditions, for example conical or profiled entry geometries or lubricated flow. For reasons based on evidence presented elsewhere [6], the most significant one being the availability of suitable test equipment, only models capable of interpreting data obtained using a flat entry geometry ($\alpha = 90^o$) have been considered, Figure 1.

The converging flow models due to Cogswell [7], Binding [8,9] and Gibson [10] were selected from that review for consideration herein, along with a further model based on a development of the Cogswell model by Rides - see Appendix A7. Comment made from here on will be with reference to these selected models only unless otherwise specified.

The Cogswell model is the most popular model, as indicated by usage in the literature [6]. There is, however, insufficient evidence in the literature to strongly support a particular choice of one of the models of either Cogswell, Binding or Gibson, or to estimate with any reasonable confidence the level of agreement that may be obtained between converging flow and tensile stretching methods. These issues will be addressed later in Section 7.5.

5.2 Advantages and disadvantages of converging flow methods

A summary of the main advantages and disadvantages of converging flow methods is presented. This represents, in part, a comparison with tensile testing methods that can be used to generate quantitative data.

- Experimentally simple

  The necessary experimental data are simply obtained from capillary extrusion rheometry measurements, often at very little or no extra cost above that needed to obtain shear viscosity data.

- Difficulty in interpreting data

  The difficulty is in the development of the appropriate converging flow models that necessarily require assumptions to be made in order to interpret the experimental data in terms of extensional viscosities. The process of calculating extensional viscosities, given a converging flow model, is itself not particularly difficult.

- Assumes equilibrium extensional viscosity behaviour

  For polymer melts the behaviour in extension is normally transient, i.e. a function of strain and time, see Figure 3. However, in the converging flow models equilibrium extensional viscosity behaviour is assumed which is thus a limitation of the method. This discussed in greater detail in Section 5.4.1.

- Very high strain rates possible

  Strain rates are typically a factor of ten smaller than the corresponding shear rates of the capillary die extrusion test. They are however considerably higher than can be achieved using tensile testing methods that tend to have an upper limit of approximately 10 s^{-1} at best.

- Cannot be used easily to determine strain hardening behaviour

  The models assume equilibrium extensional viscosities. Thus strain hardening cannot be directly deduced. The use of different contraction ratios could potentially be used to investigate strain hardening though this is considered to be fraught with complications and experimental difficulties.

- Closely mimics many processing methods

  It is preferable to use techniques that mimic the processes for which the data are being sought. In so doing the testing conditions more closely match the conditions experienced in processing, and thus the data are likely to be more relevant. The converging flow method, being an extrusion method, is widely applicable in the polymer processing sector as many processes are based on extrusion.

5.3 Comparison of the Cogswell, Rides, Gibson and Binding viscous and viscoelastic converging flow models

The basic principle behind converging flow measurements is that the pressure drop in a contraction flow is due to both the shear and extensional flow properties of the material. Thus given the pressure drop - flow rate relationship for a specified geometry and the shear flow behaviour of the material the extensional flow behaviour can be deduced.

The models due to Cogswell [7] Binding [8,9] and Gibson [10] are the most widely used models reported in the literature. The model developed by Rides [Appendix A7] is a development of the Cogswell model. The key features of these models is presented in the Table below. Equations to enable the implementation of these models are presented in Appendices A3 - A7.

Author (date)	Model type	Viscosity laws
Cogswell (1972) [7], Appendix A3	free convergence and constrained convergence	Constant extensional viscosity λ and power-law shear viscosity η
Rides (1998) Appendix A7	free convergence	Independent power-laws for extensional viscosity λ and shear viscosity η
Binding (1988) [8], Appendix A5	free convergence	Independent power-laws for extensional viscosity λ and shear viscosity η, purely viscous analysis
Binding (1991) [9], Appendix A6	free convergence	Independent power-laws for extensional viscosity λ and shear viscosity η, viscoelastic (N_1)
Gibson (1989) [10], Appendix A4	constrained or free convergence	Independent power-laws for extensional viscosity λ and shear viscosity η

Note: Free convergence indicates an entry angle $\alpha = 90°$, constrained convergence indicates $\alpha < 90°$.

In comparing the formulation of these models the observations presented as follows were made.

Gibson [10], Binding [8,9] and Rides [see Appendix A7] assumed fully independent power-law equations to describe the shear and extensional viscosities whereas Cogswell [7] assumed that the shear viscosity was defined using a power-law but that the extensional viscosity was constant.

To determine the shear component of flow each assumed a fully developed shear flow velocity profile for their analyses. However, Gibson [10] used a spherical coordinate system (as opposed to cylindrical coordinates) in order to describe the flow field with the consequence that a different "fully developed" velocity profile to that of the other models was obtained (the centre line velocity was greater in the Gibson model). With the exception of the Binding model, average strain rates were adopted in the formulation of these converging flow models. Thus Gibson, Cogswell and Rides (following Cogswell's approach) departed from the fully developed shear flow velocity profile assumption in this respect. Binding however calculated the local value of the strain rate from the assumed velocity profile.

To determine the relationship between the entrance pressure drop data and extensional viscosity, and also the position of the vortex boundary for freely converging flow, Cogswell and Binding employed the principle of minimum work. The model proposed by Gibson is for application to constrained entry flow only and therefore cannot be used to predict a free convergence entrance angle. However, Gibson indicates that the model may be used with entry angles up to 90°.

The viscoelastic model developed by Binding [9] is based on the use of the first normal stress difference, generated in shear flow. The suitability of using a shear flow generated equilibrium measure of elasticity is examined in more detail in Section 5.4.8, and its effect on predictions is considered in Section 7.3.

Development of the Cogswell model by Tremblay [11] to incorporate both power-law extensional viscosity and Rabinowitsch-corrected shear viscosity behaviour is considered to be invalid.

For further details of these models see the Appendices A3 - A7.

5.4 General assumptions made in using converging flow methods

In applying converging flow methods and also in comparing the results obtained with tensile stretching method result there are a number of assumptions that are made and these are discussed below.

5.4.1 Transient and equilibrium extensional viscosity behaviour - its implications for converging flow analysis

In contrast to shear flows where reference is normally made only to steady shear flow behaviour, extensional flow is best described as a transient behaviour. The extensional viscosity may vary as a function of both strain (or time) and strain rate, particularly at low values of strain. This transient behaviour is due to the continued development of the molecular orientation caused by the extensional flow field over the range of strains typically encountered in testing and processing. In comparison, in processes that are predominantly shearing flow the shear strain values tend to be significantly higher and the process is dominated by the material's steady state rather than transient shear flow behaviour. In describing the transient behaviour of materials in extension they may exhibit either an *unbounded stress growth* behaviour (for example reference 12, 13) or an *equilibrium extensional viscosity* value typically at large strains (for example references 14-16), Figure 3. An equilibrium extensional viscosity is dependent on strain rate but not on strain or time. This topic is discussed in more detail elsewhere [5].

The difficulty that arises in using converging flow models is that in their assumptions no account of strain hardening is made: the extensional flow behaviour is assumed to be purely viscous. Thus the models can only yield purely viscous behaviour. This complicates any comparison with data obtained from stretching techniques that exhibit non-equilibrium extensional viscosity behaviour (e.g Figure 3).

Nevertheless, converging flow methods characterise materials flowing in a region in which the total strain of deformation is constant and is determined by the contraction ratio. A review of stretching methods [5] indicated that where steady extensional viscosity values were obtained it was at strains above approximately 4. This is less than that normally obtained in converging flow measurements. Thus it is expected that, at best, good agreement can only be obtained when the material exhibits a steady extensional viscosity at values of strain lower than that occurring in the converging flow, and that the converging flow pressure drop is dominated by the region of flow in which the strain is greater than that necessary for steady extensional viscosity.

A comparison of converging flow methods with tensile methods, to validate the former approach, is presented in Section 7.5.

5.4.2 Strain rate

The strain rate in testing using converging flow methods is not constant: it varies over the converging flow region. In converging flow analysis the strain rate of the test is assigned as that at a particular place, normally at the entrance to the die. As discussed in Section 5.3 the strain rate may be taken to be an average over a region of the flow (Cogswell, Gibson or Rides) or evaluated at a specific point in the flow (Binding).

5.4.3 Location of pressure transducer

Binding and Walters [17] reported that the pressure drop in a contraction flow occurred over a relatively small region close to the entry of the die. This indicates that the positioning of the pressure transducer, i.e. sufficiently far upstream of the die entrance so that accurate measurements of entrance pressure drop are obtained, does not appear to be critical.

5.4.4 Bagley pressure drop

The entrance pressure drop determined using a Bagley plot is comprised of terms due to both the entry region and the exit region. Forsyth [18] commented that the exit pressure drop is usually of the order of one tenth of the entry pressure drop for polymer melts. However the exit pressure drop is difficult to determine accurately due to various experimental problems, for example due to viscous heating and pressure dependence effects. It is normally assumed that the exit pressure loss is negligible and thus the value of the pressure drop determined using the Bagley plot is used as the entrance pressure drop.

Furthermore the choice of dies has a significant effect on the resultant uncertainties in the measured entrance pressure drop data. For a discussion of the uncertainties in the determination of the entrance pressure drop in using either the Bagley plot or zero length die approach see Section 6.3.

5.4.5 Zero length dies

The use of zero length or very short dies can introduce measurement errors as such dies are prone to damage and wear and are also more difficult to manufacture and calibrate. There are further arguments concerning the effect of the die on the flow field. A zero length die may have a slightly different entry flow field to that of a finite length die due to the additional

constraint imposed by the internal wall of the finite length die. Thus extrapolation using two dies of finite length may yield slightly different entrance pressure drop values to that obtained using a zero length die.

Furthermore the choice of dies has a significant effect on the resultant uncertainties in the measured entrance pressure drop data. For a discussion of the uncertainties in the determination of the entrance pressure drop in using either the Bagley plot or zero length die approach see Section 6.3.

5.4.6 Non-isothermal, pressure dependant behaviour

It is normally assumed that the converging flow is isothermal and that viscosities are pressure independent. Cogswell [19] commented that the effects of these two factors tend to cancel each other out. The effect of viscous dissipation on pressure drop can be estimated using a work done principle [20]. However the author is unaware of any data on the pressure dependence of extensional viscosity, though it could be assumed to be the same as that for shear viscosity for which limited data exist [21].

5.4.7 The use of restrictive or "simple" constitutive equations

In formulating the relationship between the entrance pressure drop data and the rheological properties assumptions are necessarily made. The shear and extensional viscosity data are assumed to fit simple constitutive equations, normally power-law models (see Section 5.3).

5.4.8 Elasticity

The effect of elasticity, characterised in shear, on converging flows was reviewed elsewhere [6] and the reader is referred there for further information. In summary, on the basis of experimental and numerical work it appears that elasticity, characterised as a first normal stress difference N_1 using shearing flow methods, normally reduces the magnitude of the entrance pressure drop for polymer melts. However, the magnitude of the effect is not clearly known although evidence suggests that typically it will be small. The effect of elasticity on predictions is assessed in Section 7.3.

5.4.9 Assumed velocity field

In each of the models the velocity field in the converging flow region is assumed and is based on shear flow assumptions only for determination of the shear flow component of the pressure drop and also for determining the strain rates in the Binding model. However, in the

Cogswell, Gibson and Rides models average strain rates across the section are used. These are obviously approximations to the behaviour of polymer melts that, in reality, are likely to be far more complex in a shear and extensional flow field [22].

5.4.10 Inertia

Inertia is normally assumed to be negligible although formulation of the Binding viscous converging flow model [8] has taken it into account. For polymer melts the magnitude of the effect is considered to be negligible.

6 Measurement of entrance pressure drop and shear viscosity data

6.1 General

The data required for converging flow analysis to determine extensional viscosity values are:

- entrance pressure drop versus flow rate, and
- shear viscosity versus shear rate.

These data can be obtained using capillary extrusion rheometry, Figure 1. The international standard ISO 11443: Plastics - Determination of the fluidity of plastics using capillary and slit die rheometers [1] presents the procedure for carrying out capillary extrusion rheometry measurements on polymer melts. The reader is referred to that standard for details of the measurement technique and procedure.

In summary the capillary extrusion method involves the extrusion of polymer melt through at least two dies of different length at various flow rates (the diameter and entry geometry of the dies being the same). From measurements of the extrusion pressure, flow rate and dimensions of the dies the shear viscosity and entrance pressure drop can be determined. The theory behind the analysis is now presented.

6.2 Theory to the analysis of capillary extrusion rheometry data

By definition, shear viscosity η is the ratio of shear stress τ to shear-rate $\dot{\gamma}$

$$\eta = \frac{\tau}{\dot{\gamma}} \qquad (6.1)$$

The assumption is made that the fluid obeys a power-law relationship between shear stress and shear-rate

$$\tau \ \alpha \ \dot{\gamma}^{n} \tag{6.2}$$

where n is constant. Combining Equations 6.1 and 6.2 yields

$$\eta \ = \ \eta_o \ \dot{\gamma}^{n-1} \tag{6.3}$$

where η_0 is constant for a given temperature. The temperature dependence of shear viscosity contained in the term η_0 may be modelled using an Arrhenius type expression

$$\eta_o \ = \ \eta_o^* \ e^{k/\theta} \tag{6.4}$$

where η^*_0 and k are constant and θ is temperature. Thus the shear viscosity power-law model, Equation 6.3, can be rewritten as

$$\eta \ = \ \eta_o^* \dot{\gamma}^{n-1} \ e^{k/\theta} \tag{6.5}$$

For flow along a capillary die of length L and radius R_o, a balance of forces acting on the fluid in the die yields the relation

$$\tau_w \ = \ \Delta P/(2L/R_o) \tag{6.6}$$

where ΔP is the pressure drop along the die length L (but does not include the entrance pressure drop component) and τ_w is the shear stress acting on the fluid at the die wall [23].

To determine the wall shear stress τ_w and entrance pressure drop P_{ent} the capillary die rheometry results are collected together in the form of a Bagley plot [24] of extrusion pressure versus capillary die length-to-radius ratio L/R, for example Figure 2. Using the concept of the Bagley plot the following terms can be deduced.

Apparent wall shear stress:

The gradient x of a best-fit line to data obtained at the same flow rate is equal to $\Delta P/(L/R)$ that is equivalent to twice the wall shear stress (Equation 6.6).

$$\tau_w = \frac{x}{2} = \frac{1}{2}\left(\frac{\Delta P}{L/R}\right) \tag{6.7}$$

Entrance pressure drop:

The intercept of the best-fit line to data obtained at the same flow rate with the extrusion pressure axis, i.e. at a value of $L/R_o = 0$, yields the entrance pressure drop P_{ent}.

Apparent shear rate:

The shear-rate at the capillary die wall $\dot{\gamma}_w$ for a Newtonian fluid is given by the expression

$$\dot{\gamma}_w = \frac{4Q}{\pi R_o^3} \tag{6.8}$$

This is equivalent to the apparent shear rate $\dot{\gamma}_{ap}$ for a non-Newtonian fluid under identical test conditions of volume flow rate and die radius.

Apparent shear viscosity:

For a non-Newtonian fluid an apparent shear viscosity η_{ap} is defined by the expression

$$\eta_{ap} = \sigma_w / \dot{\gamma}_{ap} \tag{6.9}$$

where $\dot{\gamma}_{ap}$ the apparent wall shear-rate. Thus the apparent shear viscosity can be rewritten as

$$\eta_{ap} = \tau_w / \left[\frac{4Q}{\pi R_o^3}\right] \tag{6.10}$$

Thus, having obtained the wall shear stress from a Bagley plot, the apparent shear viscosity for a given flow rate can be determined.

Rabinowitsch corrected shear rate:

Assuming an apparent shear viscosity power-law behaviour

$$\eta_{ap} = \eta_{o,ap} \dot{\gamma}_{ap}^{n-1} \quad (6.11)$$

the value of $n - 1$ can be determined from the gradient of a plot of log(apparent shear viscosity) versus log(apparent wall shear rate) and $\eta_{o,ap}$ from the value of viscosity at $\dot{\gamma}_{ap} = 1 s^{-1}$.

For a power-law fluid the true shear-rate $\dot{\gamma}$ at the die wall for flow in a cylindrical die (based on the true velocity profile of a power-law fluid rather than on that of a Newtonian fluid) is given (following Rabinowitsch [25]) by

$$\dot{\gamma} = \left[\frac{3n+1}{4n}\right] \frac{4Q}{\pi R_o^3} = \left[\frac{3n+1}{4n}\right] \dot{\gamma}_{ap} \quad (6.12)$$

Rabinowitsch corrected shear viscosity:

Hence, from the definition of shear viscosity, Equation 2.1, the true shear viscosity η is given by

$$\eta = \frac{\tau_w}{\dot{\gamma}} = \left[\frac{4n}{3n+1}\right] \eta_{ap} \quad (6.13)$$

Thus, by applying the Rabinowitsch correction factor $(3n + 1)/4n$ to the apparent shear-rate and shear viscosity data (Equations 6.11 ands 6.12) true values can be obtained.

It is noted that the power-law equation for apparent shear viscosity, Equation 6.11, can be used for either apparent or true values providing consistency is maintained, although the value of the pre-exponent ($\eta_{o,ap}$ in the apparent case) will be different. Substituting apparent for true terms of shear viscosity and shear-rate in the equation

$$\eta = \eta_{o,t} \dot{\gamma}^{n-1} \quad (6.14)$$

yields the relationship

$$\eta_{o,t} = \left[\frac{4n}{3n+1}\right]^n \eta_{o,ap} \qquad (6.15)$$

where the subscript t has been used, for clarity, to indicate the true values.

6.3 Experimental procedure

The reader is referred to the international standard ISO 11443: Plastics - Determination of the fluidity of plastics using capillary and slit die rheometers [1] for the procedure for carrying out capillary extrusion rheometry measurements on polymer melts. The following presents brief details of capillary extrusion rheometry measurements and details specific to the determination of extensional viscosity data using converging flow analysis and how to improve that determination.

The basic experimental procedure is:

A1. Material is forced at various predetermined flow rates Q through a capillary die of length L and radius R_o, at constant temperature θ.

A2. The extrusion pressure P is measured upstream of the die at each flow rate.

A3. Clauses A1 and A2 are then repeated using at least one other capillary die of different length but of the same diameter and entry geometry and at the same test temperature and flow rates.

The selection of the capillary die lengths and their diameter are influenced by various factors, for example the type of material to be tested e.g. whether it is filled or unfilled, the shear rates at which data are required, the physical constraints of the extrusion rheometer, the extrudability of the material and the desired accuracy of the results. Bearing these factors in mind, the following discussion highlights indicates factors in selecting the appropriate dies to minimise the error and uncertainty in measurements.

By using at least two dies of different length but of the same diameter and entry geometry the pressure drops in (i) the converging region upstream of the die and (ii) along the die length (shear flow only) can be separately determined following the approach initially proposed by Bagley [24]. The pressure drop in the converging region upstream of the die is called the

entrance pressure drop, and the pressure drop along the length of the die bore is that due to shear flow from which the shear viscosity is determined.

Alternatively, to determine the entrance pressure drop a "zero" length die may be used. The term "zero" length die indicates a very short die such that the pressure drop obtained does not differ significantly from that of the true entrance pressure value. The extrusion pressure value obtained for that die may be then taken as the entrance pressure drop. However, to determine extensional viscosity data shear viscosity data for the material are also required thus requiring measurements using a die of at least one other length.

The use of only two dies permits the determination of the entrance pressure drop and shear viscosity values but does not yield data on the likely scatter in values. This can only be obtained by using three or more dies, or by repeat measurements using both of the dies.

The use of at least four dies of different length (or three dies with repeat measurements) allows an assessment of the linearity of the Bagley plot. This plot may be non-linear due to the effects of viscous heating and pressure dependence of viscosity. In using only three dies the magnitude of these effects cannot be assessed as the effects cannot be separated from experimental scatter.

When using only two dies, the dies should be of a sufficient difference in length to ensure sufficient accuracy of the determination of the shear viscosity and entrance pressure drop. ISO 11443 indicates that the two dies should be of $L/D \leq 5$ and $L/D \geq 20$ provided that it has been demonstrated that the Bagley plot is not significantly non-linear.

The percentage error associated with the extrusion pressure measurement is dependant on the magnitude of the pressure compared with the range on the transducer. Extrusion pressure drop values obtained for a "zero" length die are normally small and if a single pressure transducer is used for all measurements then the absolute error associated with that pressure reading can be large. The use of a non-zero length die will reduce the percentage error in that reading, but will require extrapolation of the extrusion pressure data to obtain entrance pressure drop value.

"Zero" length or very short dies are more prone to damage than longer dies, particularly if testing abrasive or filled materials. The effect of damage on the performance of a short die can be significant. It is critical to know the diameter of the die accurately. The use of very short dies may make it difficult to determine easily the diameter of the die to sufficient accuracy without potentially damaging the die. Dies for which this may be a problem are therefore not recommended.

Analysis of the uncertainties in determining entrance pressure drop data using a Bagley plot or the short or "zero" length die approach is presented in Appendix 2. The analysis is carried out on the basis of the experimental data presented in the Bagley plot in Figure 2. The results of the analysis are tabulated in Table 1. Analysis of the uncertainties in the determination of shear viscosity are presented elsewhere [26].

The difference in uncertainties in entrance pressure drop value of using a long die and either a 1 mm short die or a 5 mm short die and extrapolating to a zero length were shown to be negligible, Table 1. However, assuming that the entrance pressure drop data are the same as that obtained using a 1 mm length die can result in considerable differences (up to $\approx$ 40%) between that value and the value obtained by extrapolating to a true die length of zero. Even using a die length of 0.1 mm results in a difference in entrance pressure drop values of $\approx$ 3% - 4% from that obtained by extrapolating to a zero length. This error easily outweighs the small benefit of the reduced uncertainty in assuming that the entrance pressure drop is equivalent to the short die value rather than by extrapolation using a Bagley plot.

In conclusion, the use of "zero" length or very short dies to obtain entrance pressure drops is not recommended as they are potentially more prone to damage than longer dies and the error in the entrance pressure drop value obtained using a short die can be significant. The uncertainty analysis presented in Appendix 2 can be easily used to determine the uncertainties in an experimental set-up thereby allowing the user to estimate and minimise the errors of the experimental set-up.

6.4 Analysis of experimental results

If using at least two dies (neither one being of "zero" length) then:

A4. For each flow rate Q plot the extrusion pressure P against the die length/radius ratio (L/R_o), Figure 2. These plots are referred to as Bagley plots.

A5. The apparent shear stress is calculated as a half of the gradient of the Bagley plot, and is determined separately for each flow rate Q, Equation 6.7.

A6. The entrance pressure drop is given by the intercept value at $L/R_o = 0$ of the Bagley plot, and is determined separately for each flow rate Q.

Or, if using a "zero" or short length die as one of the dies then:

A7. For each flow rate Q plot the extrusion pressure P versus die length/radius ratio (L/R_o), Figure X. At least two dies must be used. These plots are referred to a Bagley plots.

A8. The entrance pressure drop is equivalent to the pressure drop obtained using the "zero" or short length die, and is determined for each flow rate Q.

When using a short length die, as opposed to a true length of zero, this value should be compared with that obtained by using the method in A7 using the true L/R value of the die and extrapolating to $L/R_o = 0$ to establish the level of error incurred by assuming the entrance pressure drop is the same as the extrusion pressure obtained using the short die.

A9. The apparent shear stress is calculated as a half of the gradient of the Bagley plot, and is determined separately for each flow rate Q, Equation 6.7.

Calculation of shear rates and shear viscosities:

A10. Calculate the apparent shear rate corresponding to each flow rate, Equation 6.8.

A11. Calculate the apparent shear viscosity for each apparent shear rate, Equation 6.10.

A12. Plot log(apparent shear viscosity) versus log(apparent shear rate) and determine the gradient of the plot which is equivalent to n-1. Thus n can be determined.

A13. Calculate the Rabinowitsch corrected or true shear rate and shear viscosity values as necessary, Equations 6.13 and 6.12 respectively.

Analysis of entrance pressure drop and shear viscosity data

A14: The entrance pressure drop and shear viscosity data can be analysed using the converging flow models as detailed in Appendices A3 - A7.

A15: The models assume power-law behaviour for shear viscosity as a function of shear rate and entrance pressure drop as a function of flow rate. However the experimental data may not fit such power-laws reasonably well. If this is the case then it may be desirable to split the data into two or more ranges over each of which the data are

reasonably fitted by a power-law. These ranges of data can then be analysed separately. Assessment of the effect of variations in the input data on predictions indicates that this is more important for entrance pressure drop data than shear viscosity data.

6.5 Uncertainties in the measured data

An intercomparison of shear viscosity and entrance pressure drop measurements by capillary extrusion rheometry that was based on ISO11443 was carried out to determine the precision of capillary extrusion rheometry data [26]. The following precision data were determined from that intercomparison comprising of 20 laboratories in total on a high density polyethylene (HDPE) and a glass-fibre filled polypropylene (GFPP).

Table: Extrusion pressure measurement

Material, test temperature	HDPE, 190 °C	GFPP, 230 °C
Repeatability (1 standard deviation)	7.0%	13.4%

Table: Shear viscosity measurement (Rabinowitsch corrected for entrance pressure drop and non-Newtonian velocity profile)

Material, test temperature	HDPE, 190 °C	GFPP, 230 °C
Repeatability (1 standard deviation)	7.2%	8.6%
Reproducibility (1 standard deviation)	9.9%	12.2%

Table: Entrance pressure drop measurement

Material, test temperature	HDPE, 190 °C contraction ratio of 15 only	HDPE, 190 °C contraction ratios 9.55 -15.5	GFPP, 230 °C contraction ratio of 15 only
Reproducibility (1 standard deviation)	15.1%	17.8%	19.8%

Note: The contraction ratios presented here are barrel diameter to die diameter ratios.

Data obtained for the shear viscosity and entrance pressure drop of the HDPE are shown in Figures 10 and 11 respectively.

The most major sources of error were considered to be due to accuracy of pressure measurement and utilisation of the pressure transducer in the appropriate range. In testing in accordance with the specification of the standard ISO 11443 the uncertainties in the measurement of shear viscosity were estimated to be in the range 2.5 - 19% for the polyethylene and polypropylene materials, and depended most significantly on the range over which the pressure transducer was being used [26].

The choice of die lengths and whether to use a "zero" length die will obviously affect the accuracy of the determined entrance pressure drop and shear viscosity values. An analysis of the uncertainties of the determination of entrance pressure drop, based on the uncertainties of pressure measurement, are presented in Appendix 2. This may be used to assess the errors associated with the particular material and pressure transducer. It is noted that these uncertainties are already contained in the experimental precision data presented above and are not additional to it.

7 Example experimental data for polymeric materials

7.1 General

Section 7 of this document is aimed at illustrating various aspects of the use and validity of converging flow methods for determining extensional viscosity data. It covers:

- an examination of the experimental determination of entrance pressure drop and shear viscosity data, Section 7.2,
- an intercomparison of the predictions of the various converging flow models, Section 7.3,
- an assessment of the effect of uncertainties in input data on predicted extensional viscosity values, Section 7.4, and
- a comparison of the predictions of the models with data obtained using a tensile stretching method, Section 7.5.

7.2 Experimental data: entrance pressure drop and shear viscosity determination

A typical Bagley plot of extrusion pressure versus die length to radius ratio for a high density polyethylene is shown in Figure 4. The plot illustrates that at small L/R_o values the extrusion pressure is small. At the highest apparent shear rate, for the datum at $L/R_o = 5$ the pressure is approximately one quarter of that at $L/R_o = 30$. In using a die of $L/R_o = 1$ it would be approximately one seventh illustrating the problems with the accuracy of pressure measurement when using short dies. The plot is reasonably linear. However an improved fit to the data can be obtained by using a second order polynomial, Figure 5 and Table 2. This difference in fit, although appearing quite small, produces a significant difference in the entrance pressure drop values obtained. At the highest flow rate, fitting the data using a second order polynomial increased the entrance pressure drop by 21%, and at the lowest rate by 6%, Table 2. The use of the polynominal to fit the data also indicates, and quantifies, a variation in viscosity (proportional to the gradient of the curve) that is possibly due to a pressure dependence of the material. The differences in the entrance pressure drop and shear viscosity between using a linear fit and a polynomial fit are shown in Table 2. In using this data in a converging flow analysis the decrease in shear viscosity and the increase in entrance pressure drop will both have the same effect of increasing the predicted extensional viscosity, estimated to be of the order of 30% by using Table 5.

The effect of fibres on the entrance pressure drop can be very significant, Figures 6. For this material, containing 15% by weight of long glass fibres, the entrance pressure drop is of the order of 50% - 60% of the extrusion pressure drop for a die of $L/R = 30$, compared with 10% - 15% for the HDPE, Figure 4. The effect of differences in the length of the glass fibres has no significant effect on the measured shear viscosity, Figure 7. However, they did have a significant effect on the measured entrance pressure drop values, Figure 8. This clearly demonstrates that entrance pressure drop measurements, and thus extensional viscosity measurement, can be a more sensitive measure of material consistency or batch-to-batch variation that is not clearly revealed through shear viscosity measurements.

7.3 Intercomparison of the predictions of the various models

The predicted extensional viscosity data using the various models and raw entrance pressure drop and shear viscosity data are presented for various materials to illustrate how the predictions of the models compare:

- glass fibre filled unsaturated polyester dough moulding compound DMC L7049 at 50 °C: Figures 6 - 9.

- high density polyethylene HFU000 at 190 °C: Figures 10 - 12 and Table 3.
- a glass fibre filled polypropylene HFQ000 at 230 °C - extensional viscosity data only: Figure 13 and Table 3.
- high density polyethylene HFU000 at 150 °C: Figures 14 - 16.
- low density polyethylene - HGE000 at 150 °C: Figures 14 - 15, 17.
- linear low density polyethylene - HGF000 at 150 °C: Figures 14 - 15, 18.

The NPL references to the materials, e.g. HFU000, are used to identify the different grades of materials.

As an example of such a comparison, the predictions of the models for the unsaturated polyester dough moulding compound are shown in Figure 9. This plot shows that the Cogswell model predicts extensional viscosity values ≈ 100% higher than values predicted using the Binding and Rides models, and ≈ 160% higher than those predicted using the Gibson model. Extensional viscosity values predicted using the Cogswell model are of the order of x100 that of the shear viscosity values.

The extensional viscosities of the HDPE and glass-filled PP materials used in the capillary extrusion rheometry intercomparison [26] are presented in Figures 12 and 13. The shear viscosity and entrance pressure drop data for the HDPE are shown in Figures 10 and 11 respectively, and illustrate the variability in data obtained using capillary extrusion rheometry.

The extent to which the Cogswell model predicts higher extensional viscosity values compared with the Gibson and Rides models appears to depend on the magnitude of the extensional viscosity power law exponent m, Figures 9, 12-13, 16-18. Typically, the lower the value of m the more the predictions of the Gibson, Binding and Rides models agree with each other and disagree with the predictions of the Cogswell model. Such a difference between the Cogswell and Rides models is not unexpected as the difference in their formulation is the incorporation of a rate dependent extensional viscosity in the latter. Obviously the effect of this would only be apparent when there is a rate dependence of extensional viscosity, and its effect would be expected to increase as the magnitude of the rate dependence increased.

It is proposed that the difference between the predictions of the Binding model and the Cogswell, Gibson and Rides models for high values of m is related to the assumptions made in formulating the models concerning the strain rate. In the Binding model the strain rate is evaluated everywhere based on the shear flow velocity profile whereas the other models use average strain rate values. It is hypothesised that for a material exhibiting a constant extensional viscosity (m = 1) the velocity field would adopt a profile to reduce the maximum strain rates more so than for a material that exhibited strain rate thinning (low m value). The

basis for this is that a high viscosity, high strain rate flow corresponds to a large dissipation of energy and thus a large pressure drop (the energy dissipated is proportional to the product of the viscosity and the rate raised to the power 2). The flow will tend to optimise its velocity profile to minimise the pressure drop. The consequence of this is that the flow will adopt a profile that minimises the maximum strain rates thus approximating more closely to the assumed average extension rate of the Cogswell, Gibson and Rides models. For a strain rate thinning material the energy dissipated by a low rate, high viscosity flow is more similar to that dissipated by a high rate, low viscosity flow and thus such a rearrangement of the velocity profile is not so necessary and the difference in the dissipated energy, and thus pressure drop, due to the different assumed strain rate profiles is less. The consequence is that for strain rate thinning materials the models predict similar extensional viscosities.

In comparing the models the predictions of the Gibson model appear to be most variable. In all cases the order of decreasing magnitude of predictions was Cogswell, Rides and then Binding, whereas the Gibson model yielded both the lowest and the highest extensional viscosities, Figures 9 and 17 respectively.

The use of the Binding viscoelastic model, compared with the Binding viscous model, resulted in a negligible difference in the predictions of extensional viscosity, Figures 12 and 13 and Table 4. The differences in predicted values between the Binding viscous and viscoelastic models in the inelastic cases (test references 45 and 46 in Table 4) is due to the fact that a term to take into account a contraction ratio effect that is included in the viscous model is not included in the viscoelastic model. The effect of this term is small, of the order of 3% for the HDPE and 1% for GFPP, but should be taken into account. Thus the true effect of elasticity is of the order of 3% for HDPE and 1% for GFPP. Thus these results indicates that the incorporation of viscoelasticity based on shear flow measurement of the first normal stress difference is not necessary for polymer melts.

7.4 Assessment of the effect of uncertainties in input data on predicted extensional viscosity values

The high density polyethylene (HFU000) was used to illustrate the sensitivity of predictions to variations in the input data. Input data were increased by certain amounts and the effect on predictions recorded, Tables 3-6. In summary:

Increasing the entrance pressure drop data by 10% increased the extensional viscosity values by 16%, except for the Gibson model which was by 10%.

Increasing the shear viscosity data by 10% decreased the extensional viscosity data by 5%, except for the Gibson model which was by 1%.

Increasing the normal stress difference data by 100% had a negligible effect.

In carrying out converging flow analysis of data it is recommended that this type of analysis of the effect that uncertainties in input data have of the predicted extensional viscosity values is performed.

7.5 Comparison of the predictions of the models with data obtained using a tensile stretching method

To assess the validity of the converging flow approach for determining extensional viscosity data a comparison of data obtained by converging flow with that obtained using a tensile testing method [27] has been made. Three materials: a high density polyethylene, a low density polyethylene and a linear low density polyethylene were chosen as they exhibited quite different strain hardening characteristics, Figure 3. The shear viscosity data and entrance pressure drop data for the materials are presented in Figures 14 and 15 respectively. Predictions obtained using the converging flow models are presented in Figures 16 - 18. The LDPE has the highest ratio of extensional to shear viscosity values, being of the order of at least $\approx$ x 10 and compares with a value of at least $\approx$ x 7 for the HDPE (both comparing shear viscosity with the predictions of the Binding model). The extensional viscosity of the LLDPE is the least strain rate dependent, and has the lowest value of the ratio of extensional to shear viscosity of less than 4 (again comparing shear viscosity with the Binding prediction of extensional viscosity). Comparison with the Cogswell model will result in higher ratios being obtained.

As discussed in Section 5, and in particular in 5.4.1, there are considerable difficulties in comparing data from converging flow analyses with those from tensile stretching methods, principally due to the transient nature of the extensional viscosity behaviour.

A simple approach is to compare the converging flow predictions with the maximum value of the tensile stress growth coefficient values obtained at each strain rate, Figure 19 (The predictions of the Cogswell model have been used in this comparison. The effect of using an alternative model can be estimated by comparing with the respective plot of Figures 16-18). The comparison plotted in Figure 19 ignores the potential effect that the strain history may have on results. The resultant plot shows good agreement of the data from the two methods for LDPE and HDPE - to within 30 - 40%. The discrepancy for LLDPE was greater with the converging flow predictions being $\approx$ 50% lower.

An improved approach is to take account of the strain that the material has undergone in testing. In the converging flow the material undergoes a strain that is given by the natural logarithm of the area contraction ratio. For example, the Hencky strain occurring in a contraction having a 15:1 barrel to die diameter is calculated to be ≈ 5.4. Thus converging flow data have been plotted in Figures 21 - 23 along with tensile test data as a function of strain and at the same strain rates. The converging flow data have had to be interpolated or extrapolated as indicated to achieve equivalent strain rate data. These results again show quite good agreement of tensile with converging flow extensional viscosity data.

It is noted that the high degree of scatter for the LLDPE data, Figure 22, is due to the low rate, low viscosity test approaching the lower limit of the measurement capability of the tensile testing instrument.

The comparison presented above was on the basis of using the Cogswell model. For the HDPE and LDPE materials the Cogswell model generally predicted extensional viscosity values 80% higher than the other models. For LLDPE the Cogswell model predicted values of the same order as the other models, except for the Binding model in which case the predictions of the Cogswell model were 60% higher.

It is concluded on the basis of the data presented that the Cogswell model yields better agreement with the tensile stretching data than the other models.

Finally, it is noted that the shear viscosities and extensional viscosities of the materials HDPE, LDPE and LLDPE exhibit different trends. In order of decreasing shear viscosity they rank LLDPE, LDPE and then HDPE, whereas in order of decreasing extensional viscosity they rank LDPE, HDPE and then LLDPE. The latter trend is exhibited by both the converging flow and tensile stretching methods. This highlights the importance of extensional flow measurements in fully characterising the flow behaviour of materials, especially where those materials are to be used in processes in which the deformation is predominantly extensional.

8 Summary

The most widely used models, as evident in the literature [6], are those due to Cogswell [7], Binding [8] and Gibson [10] with Cogswell's being the most popular. Various aspects of the experimental determination of the shear viscosity and entrance pressure drop data needed for inputting into the converging flow models have been presented. The predictions of these

models, and a development of the Cogswell model, have been compared and their sensitivities to input data assessed.

On a theoretical basis it has been demonstrated that the constant extensional viscosity assumption made by Cogswell results in higher predictions of extensional viscosity than if the material were assumed to obey a power-law. Also, it has been hypothesised on the basis of the evidence presented that the assumptions made in defining the strain rates used in the Binding model results in the extensional viscosity being under-predicted for materials that do not exhibit a high degree of strain rate thinning. These observations indicate the potential way forward to developing an improved model for determining extensional viscosity data.

The difficulties of reliably validating these models against other methods were discussed. The principle difficulty is that the extensional viscosity of polymer melts is normally a function of strain rate and strain, whereas in the converging flow approach it is assumed to be an equilibrium value that is a function of strain rate but not strain. Nevertheless, validation of the converging flow models against a tensile stretching method is presented and indicates that good agreement can be obtained thus supporting and validating the use of converging flow models for determination of extensional viscosity values.

It was concluded that the Cogswell model yielded better agreement with the tensile stretching data than the other models assessed, despite the theoretical limitations in the model as discussed above.

Furthermore, some of the errors incurred in using a converging flow model to determine extensional viscosity data may, fortuitously, be cancelled if those data are then used to calculate the pressure drop in another flow geometry. It is recommended that the same converging flow model is used for both the analysis of entrance pressure drop data and for their application.

Despite the problems with, and limitations of converging flow methods the technique has considerable benefits as a materials characterisation method:

- it can provide valuable information on the extensional flow behaviour of melts,
- it is relatively simple to use, and
- if capillary extrusion rheometry is to be used to determine shear flow behaviour then entrance pressure drop data and thus extensional viscosity data can be obtained at minimal additional cost.

9 Acknowledgements

The work reported in this paper was carried out as part of a project on measurement of the extensional viscoelastic properties of polymers. This project is part of a programme of underpinning research financed by the Engineering, Automotive and Metals Division (EAM) of the Department of Trade and Industry on measurements related to the processability of materials.

References

1 ISO 11443:1995 Determination of the fluidity of plastics using capillary and slit-die rheometers, that defines the procedure for capillary extrusion rheometry of plastics (This standard is identical to the British standard BS2782: Part7: Method 722B: 1996).

2 Han, C.D., Rheology in Polymer Processing, Academic Press, London 1976.

3 Tanner, R.I., Engineering Rheology, Clarendon Press, Oxford, 1985.

4 Pearson, J.R.A., Mechanics of Polymer Processing, Elsevier Applied Science Publishers Ltd, London, 1985.

5 Rides, M., Allen, C.R.G., and Chakravorty, S., Review of extensional viscoelasticity measurement techniques for polymer melts, NPL Report CMMT(A)44, October 1996.

6 Rides, M. and Chakravorty, S., Review of converging flow methods for determining the extensional flow behaviour of polymer melts, NPL Report CMMT(A)80, August 1997.

7 Cogswell, F.N., Polym. Eng. Sci., 12 No.1 (1972) pp.64-73.

8 Binding, D.M., J. Non-Newtonian Fluid Mech., 27 (1988) pp.173-189.

9 Binding, D.M., J. Non-Newtonian Fluid Mech., 41 (1991) pp.27-42.

10 Gibson, A.G., Composites, 20 No.1 (1989) pp.57-64.

11 Tremblay, B., J. Non-Newtonian Fluid Mech. 33 (1989) pp.137-164.

12 Meissner, J., Trans. Soc. Rheol., 16 (1972) pp.405-420.

13 Meissner, J., Chem Eng. Commun., 33 (1985) pp.159-180.

14 Münstedt, H., J. Rheology, 23 (1979) pp.421-436.

15 Laun, H.M., and Münstedt, H., Rheol. Acta, 15 (1976) pp.517-524.

16 Laun, H.M., and. Schuch, H., J. Rheology, 33 (1989) pp.119-175.

17 Binding, D.M. and Walters, K., J. Non-Newtonian Fluid Mech., 30 (1988) pp.233-250.

18 Forsyth, T.H., Polym-Plast. Technol. Eng., 6 (1976) pp.101-131.

19 Cogswell, F.N., Polymer Melt Rheology. George Godwin Ltd, London, 1981.

20 Rides, M., Aspects of the rheology of unsaturated polyester dough moulding compounds, Ph.D Thesis, Brunel, The University of West London, January 1993.

21 Chakravorty, S., Rides, M., Allen, C.R.G. and Brown, C.S., The pressure dependency of the shear viscosity of polymer melts: an international round robin study, NPL Report CMMT(A)7, March 1996, National Physical Laboratory.

22 Barnes, H.A. and Roberts, G.P., J. Non-Newtonian Fluid Mech., 44 (1992) pp113-126.

23 Brydson, J.A., Flow Properties of Polymer Melts. George Godwin Ltd, London, Second Edition, 1981.

24 Bagley, E.B., J. Applied Physics, 28 No.5 (1957) pp.624-627.

25 Rabinowitsch , B., Z Physik. Chem., A145, 1 (1929), pp.1-26.

26 Rides, M., Allen, C.R.G., Capillary extrusion rheometry intercomparison using polyethylene and glass-fibre filled polypropylene melts: measurement of shear viscosity and entrance pressure drop, NPL Report CMMT(A)25, May 1996.

27 Rides, M., Extensional flow properties of polymer melts: their measurement and effect on processing performance, NPL Report CMMT(B)200, August 1998.

28 Rheological Techniques, R.W. Whorlow, Ellis Horwood, London, 1992.

29 Gupta, R.K. and Shridar, T., Elongational Rheometers, in Rheological Measurement, Ed. A.A. Collyer and D.W. Collyer, Elsevier Applied Science, London, 1988.

30 Dealy, J.M., Polym. Eng. Sci., 11 (1971) pp.433-445.

31 Dealy, J.M., J. Non-Newtonian Fluid Mech., 4 (1978) pp.9-21.

32 Dealy, J.M., J. Rheology 39(1) January/February 1995, pp.253-265.

33 Meissner, J., Stephenson, S.E., Demarmels A. and Portman, P., J. Non-Newtonian Fluid Mechanics, 11 (1982) pp.221-237.

34 Rheometry, K. Walters, Chapman and Hall, London, 1975.

Uncertainties in entrance pressure determination		1 mm short die				0.1 mm short die			
		fast rate		slow rate		fast rate		slow rate	
Die 1 - short die	$(L/R)_1$	5	1	5	1	5	0.1	5	0.1
Pressure 1	P_1, MPa	4	2.08	1.6	0.736	4	1.648	1.6	0.542
Uncertainty in pressure 1	p_1, MPa	0.05	0.05	0.05	0.05	0.05	0.05	0.05	0.05
Fractional uncertainty in P_1, %	100% x p_1/P_1	1.3	2.4	3.1	6.8	1.3	3.0	3.1	9.2
Die 2 - long die	$(L/R)_2$	30	30	30	30	30	30	30	30
Pressure 2	P_2, MPa	16	16	7	7	16	16	7	7
Uncertainty in pressure 2	p_2, MPa	0.05	0.05	0.05	0.05	0.05	0.05	0.05	0.05
Fractional uncertainty in P_2, %	100% x p_2/P_2	0.3	0.3	0.7	0.7	0.3	0.3	0.7	0.7
Entrance pressure by Bagley method	P_{ent}, MPa	1.6	1.6	0.52	0.520	1.6	1.6	0.52	0.520
Uncertainty in entrance pressure by Bagley method	p_{ent}, MPa	0.052	0.050	0.052	0.050	0.052	0.050	0.052	0.050
Fractional uncertainty in entrance pressure value by Bagley method	100% x p_{ent}/P_{ent}	3.2	3.1	10.0	9.6	3.2	3.1	10.0	9.6
Fractional uncertainty in using short die measurement as entrance pressure, %	100% x p_1/P_1		2.4		6.8		3.0		9.2
% error in using short die measurement as entrance pressure, %	100% x $(p_{ent}-P_1)/P_{ent}$		30		42		3		4

Slow rate: apparent shear rate = 11.6 s^{-1}
Fast rate: apparent shear rate = 86.2 s^{-1}

Table 1: Analysis of uncertainties in determining entrance pressure drop values.

True shear rate	linear			quadratic			% difference in values	
s^{-1}	gradient, n-1	intercept, MPa	R^2	gradient, n-1	intercept, MPa	R2	gradient, n-1	intercept, MPa
15.8	0.463	1.852	0.9988	0.399	2.277	0.9999	15	-21
21.4	0.405	1.599	0.9992	0.359	1.902	1.0000	12	-17
31.8	0.357	1.352	0.9995	0.326	1.551	0.9999	9	-14
43.7	0.311	1.162	0.9996	0.288	1.319	0.9999	8	-13
61.7	0.276	0.963	0.9994	0.253	1.112	0.9998	9	-14
86.1	0.233	0.867	0.9995	0.222	0.937	0.9997	5	-8
118.0	0.204	0.770	0.9998	0.196	0.819	0.9999	4	-6

Table 2: Effect of the method of analysis of the Bagley plot on entrance pressure drop values.

HDPE (HFU000, ref. 043)		m	λo Pa.s^m	λ at 10 s^{-1} Pa.s	λ at 100 s^{-1} Pa.s	λ/η at 10 s^{-1}	λ/η at 100 s^{-1}
Model:							
Cogswell		0.532	2.45E+05	8.35E+04	2.84E+04	25	32
Rides		0.532	1.51E+05	5.14E+04	1.75E+04	15	20
Binding viscous		0.532	1.16E+05	3.94E+04	1.34E+04	12	15
Gibson		0.498	1.23E+05	3.88E+04	1.22E+04	12	14
Binding viscoelastic		0.535	1.16E+05	3.96E+04	1.36E+04	12	15
η_o (Pa.s^n) =	1.25E+04		range =	4.47E+04	1.62E+04	13	18
n =	0.427		% of range	88%	95%	88%	95%

PP (HFQ000, ref. 044)		m	λo Pa.s^m	λ at 10 s^{-1} Pa.s	λ at 100 s^{-1} Pa.s	λ/η at 10 s^{-1}	λ/η at 100 s^{-1}
Model:							
Cogswell		0.858	4.18E+04	3.01E+04	2.17E+04	28	81
Rides		0.858	3.63E+04	2.61E+04	1.88E+04	24	70
Binding viscous		0.858	2.33E+04	1.68E+04	1.21E+04	16	45
Gibson		0.658	2.72E+04	1.24E+04	5.63E+03	12	21
Binding viscoelastic		0.855	2.34E+04	1.67E+04	1.20E+04	16	45
η_o (Pa.s^n) =	4.29E+03		range =	1.78E+04	1.61E+04	17	60
n =	0.398		% of range	87%	114%	87%	114%

Shear viscosity pre-exponent is Rabinowitsch corrected value.

Table 3: Comparison of predictions of the converging flow models for an HDPE and a PP.

Material		HDPE (HFU000)	HDPE (HFU000)	HDPE (HFU000)	GFPP (HFQ000)	GFPP (HFQ000)	GFPP (HFQ000)
Normal stress difference		N1≠0	N1=0	% difference	N1≠0	N1=0	% difference
Test reference		43	45	between 43 & 45	44	46	between 44 & 46
Viscous model	m_D	0.532	0.532	-	0.858	0.858	-
Viscoelastic model	m_F	0.535	0.532	0.6%	0.855	0.858	-0.3%
% difference		0.6%	0.0%	-	-0.3%	0.0%	-
Viscous model	λo_D, $Pa.s^m$	1.16E+05	1.16E+05		2.33E+04	2.33E+04	
Viscoelastic model	λo_F, $Pa.s^m$	1.16E+05	1.13E+05	2.3%	2.34E+04	2.31E+04	1.3%
% difference		-0.3%	-2.7%	-	0.3%	-1.0%	-

m_D and λo_D indicate the extensional viscosity exponent and pre-exponent respectively, predicted using the Binding viscous model
m_F and λo_F indicate the extensional viscosity exponent and pre-exponent respectively, predicted using the Binding viscoelastic model

Table 4: Effect of the elasticity term on predictions using the Binding models.

Test case description		HDPE (HFU000, ref. 043) original data		ref. 047 +10% increase in entrance pressure values		ref. 048 +10% increase in shear viscosity values	
Input data:	$P_{ent,o}$, $Pa.(m^3s^{-1})^{-s}$	1.21E+10		1.34E+10		-	
	s	0.495		-		-	
	η_o, $Pa.s^n$	1.25E+04		-		1.37E+04	
	n	0.427		-		-	
	$N1_o$, $Pa.s^{p+1}$	1.22E+04		-		-	
	p	-0.400		-		-	
Model		m	λ_o, $Pa.s^m$	m	λ_o, $Pa.s^m$	m	λ_o, $Pa.s^m$
Cogswell		0.532	2.45E+05	0.532	2.84E+05	0.532	2.33E+05
Rides		0.532	1.51E+05	0.532	1.75E+05	0.532	1.43E+05
Binding viscous		0.532	1.16E+05	0.532	1.34E+05	0.532	1.10E+05
Gibson		0.498	1.23E+05	0.498	1.36E+05	0.499	1.22E+05
Binding viscoelastic		0.535	1.16E+05	0.535	1.33E+05	0.535	1.10E+05
% change due to variation in input data							
Cogswell		-	-	0.0	15.7	0.0	-4.9
Rides		-	-	0.0	15.7	0.0	-5.0
Binding viscous		-	-	0.0	15.7	0.0	-4.9
Gibson		-	-	-0.1	10.5	0.1	-0.6
Binding viscoelastic		-	-	0.0	15.5	0.0	-4.9
Ratio λ/η		$10\ s^{-1}$	$100\ s^{-1}$	$10\ s^{-1}$	$100\ s^{-1}$	$10\ s^{-1}$	$100\ s^{-1}$
Cogswell		25	32	29	37	24	30
Rides		15	20	18	23	15	19
Binding viscous		12	15	14	17	11	14
Gibson		12	14	13	15	12	14
Binding viscoelastic		12	15	14	18	11	15

Table 5: Sensitivity of the predictions of the converging flow models to variations in the input data - I.

Test case description		HDPE (HFU000, ref. 043) original data		ref 049 +100% in N1 value		ref. 050 changing entrance pressure parameters by 2 s.d.		ref. 051 changing shear viscosity parameters by 2 s.d.	
Input data:	$P_{ent,o}$, Pa.$(m^3s^{-1})^{-s}$	1.21E+10		-		2.55E+10		-	
	s	0.495		-		0.537		-	
	η_o, Pa.s^n	1.25E+04		-		-		1.44E+04	
	n	0.427		-		-		0.366	
	$N1_o$, Pa.s^{p+1}	1.22E+04		2.44E+04		-		-	
	p	-0.400		-		-		-	
Model		m	λ_o, Pa.s^m	m	λ_o, Pa.s^m	m	λ_o, Pa.s^m	m	λ_o, Pa.s^m
Cogswell		0.532	2.45E+05	-	-	0.604	2.04E+05	0.569	2.29E+05
Rides		0.532	1.51E+05	-	-	0.604	1.36E+05	0.569	1.47E+05
Binding viscous		0.532	1.16E+05	-	-	0.604	1.01E+05	0.569	1.07E+05
Gibson		0.498	1.23E+05	-	-	0.542	1.09E+05	0.502	1.22E+05
Binding viscoelastic		0.535	1.16E+05	0.538	1.18E+05	0.606	1.01E+05	0.570	1.05E+05
% change due to variation in input data									
Cogswell		-	-	-	-	13.5	-16.9	7.0	-6.7
Rides		-	-	-	-	13.5	-10.0	7.0	-2.7
Binding viscous		-	-	-	-	13.5	-13.2	7.0	-7.8
Gibson		-	-	-	-	8.8	-11.5	0.7	-1.3
Binding viscoelastic		-	-	0.6	2.4	13.3	-12.3	6.6	-9.2
Ratio λ/η		10 s^{-1}	100 s^{-1}	10 s^{-1}	100 s^{-1}	10 s^{-1}	100 s^{-1}	10 s^{-1}	100 s^{-1}
Cogswell		25	32	-	-	25	37	25	35
Rides		15	20	-	-	16	25	16	23
Binding viscous		12	15	-	-	12	18	12	17
Gibson		12	14	-	-	11	15	12	14
Binding viscoelastic		12	15	12	16	12	19	12	16

Table 6: Sensitivity of the predictions of the converging flow models to variations in the input data - II.

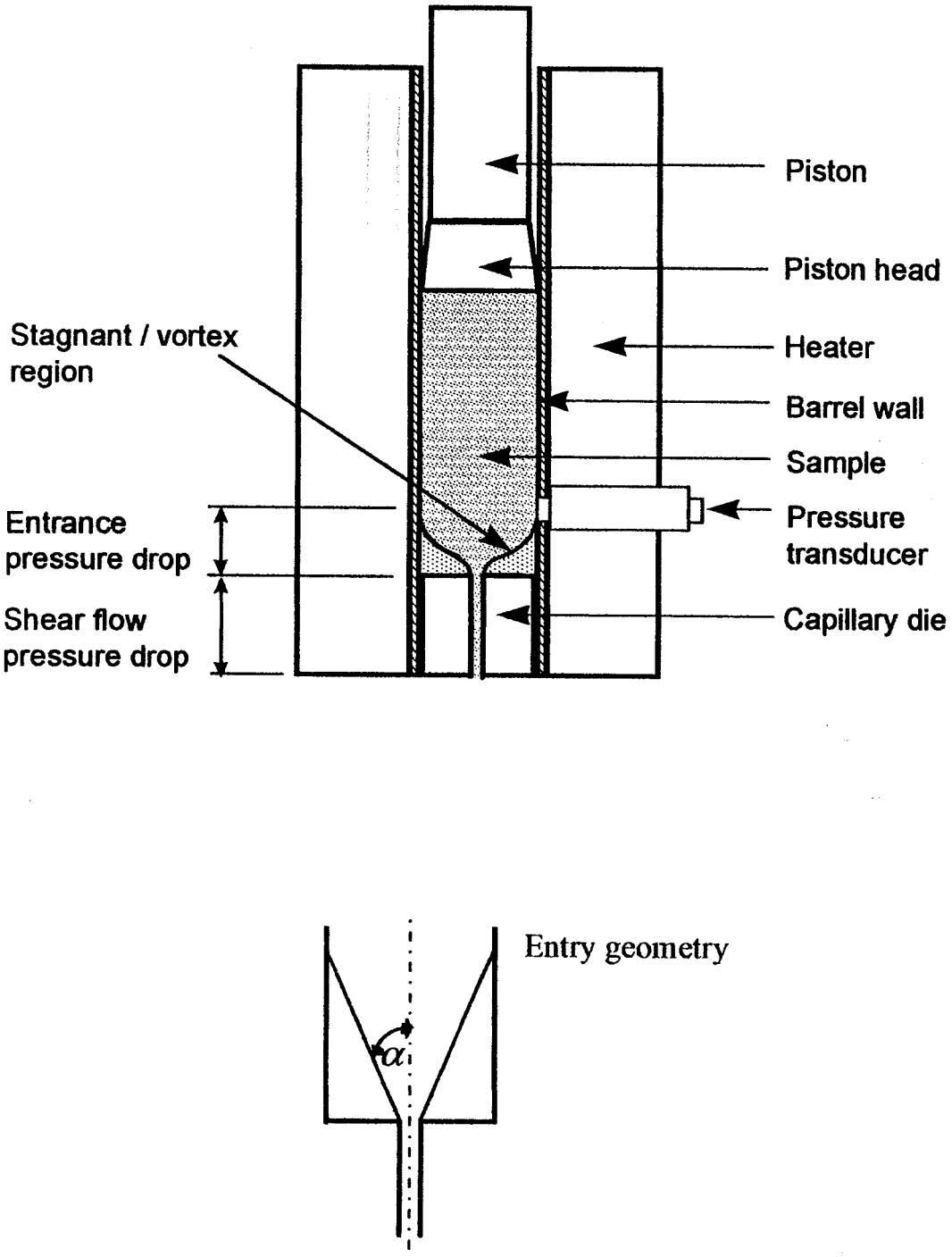

Figure 1: Converging flow in a capillary extrusion rheometer.

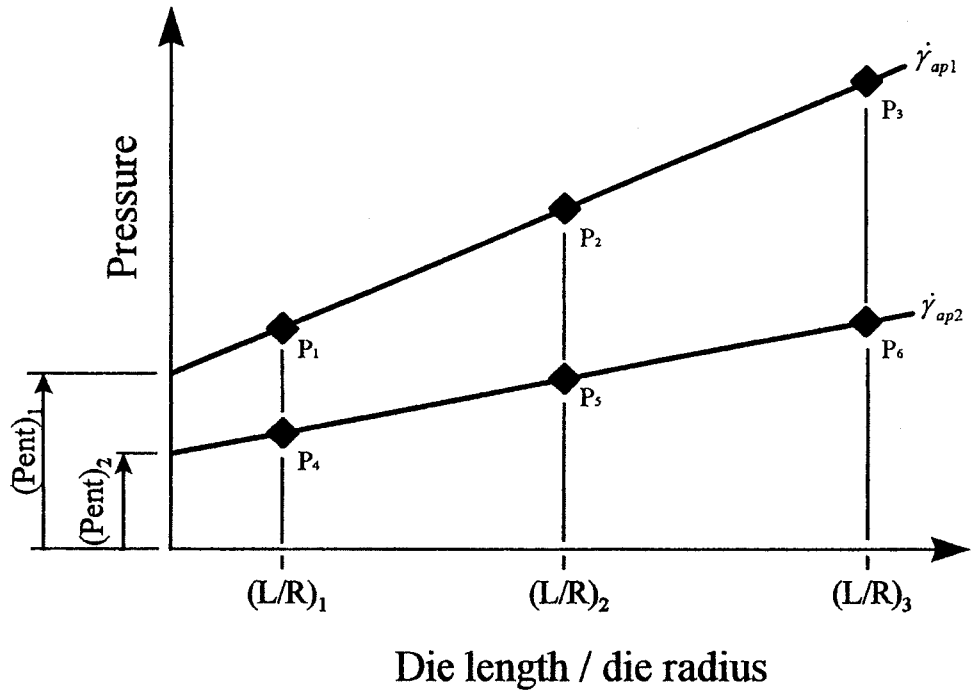

Figure 2: Bagley plot used for the determination of entrance pressure drop and shear viscosity.

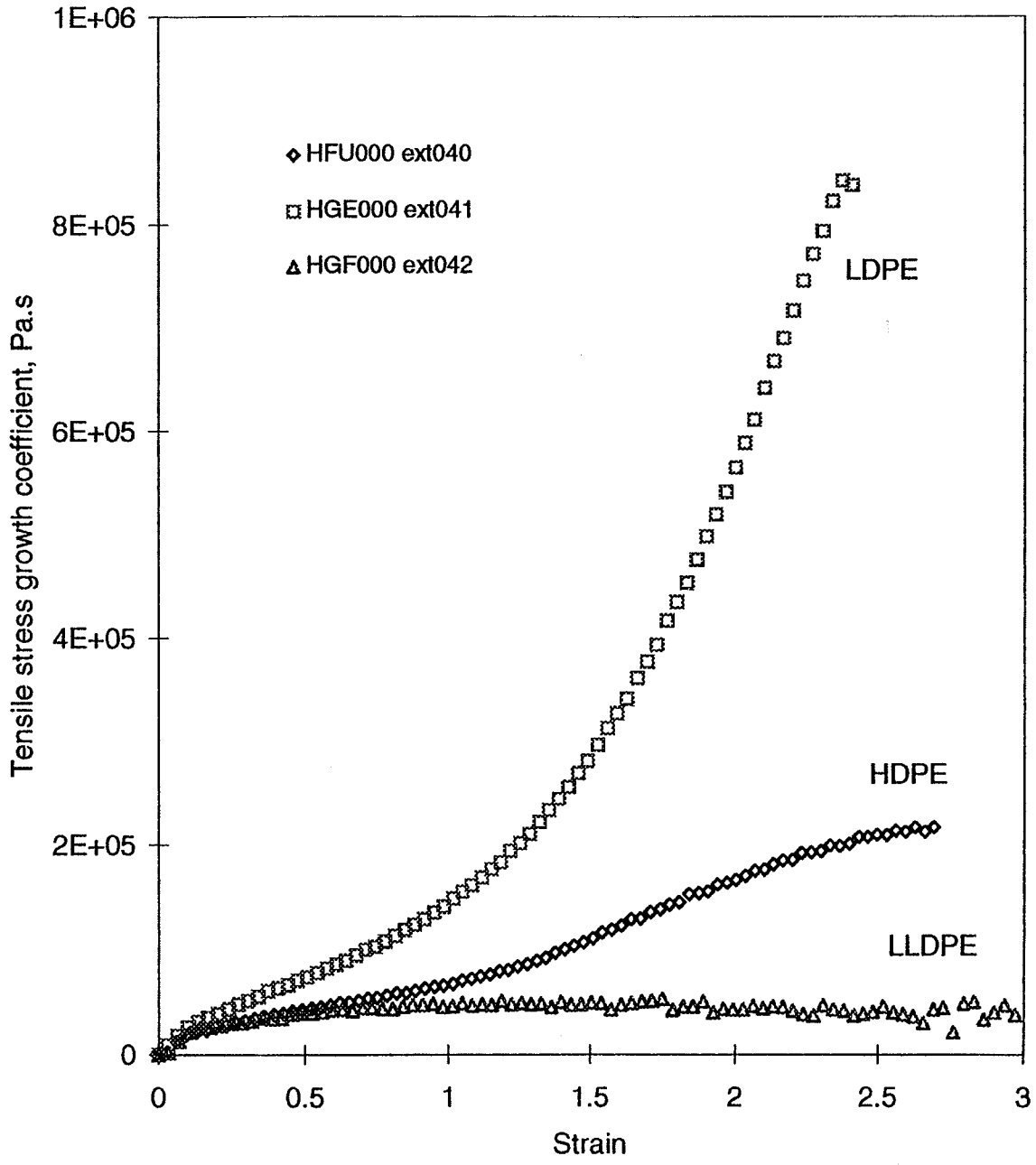

Figure 3: Strain hardening behaviour of three polymer melts measured at a strain rate of $\approx 0.7\ s^{-1}$ and at 150 °C.

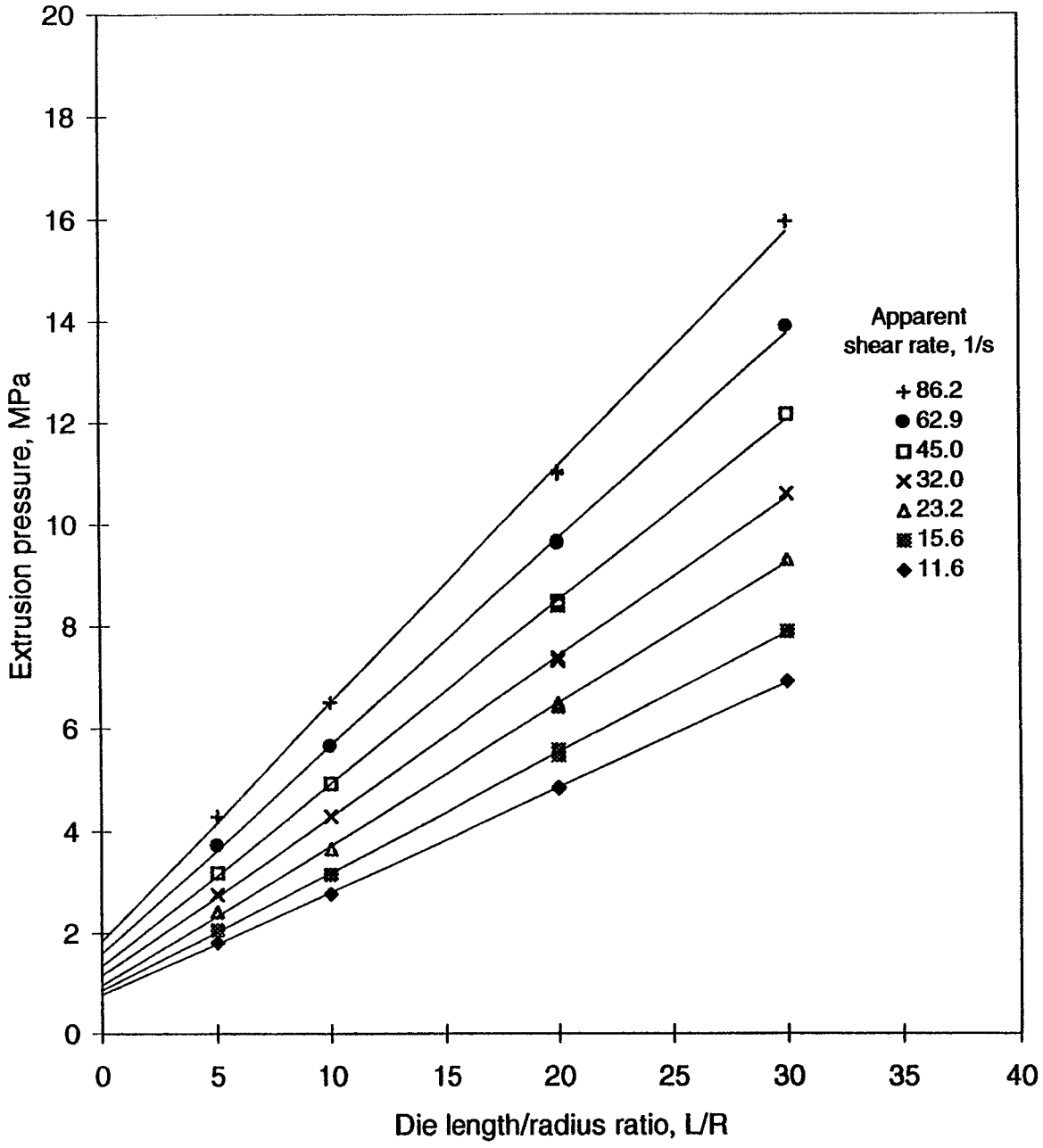

Figure 4: Typical Bagley plot for an HDPE (HFU000) at 190 °C.

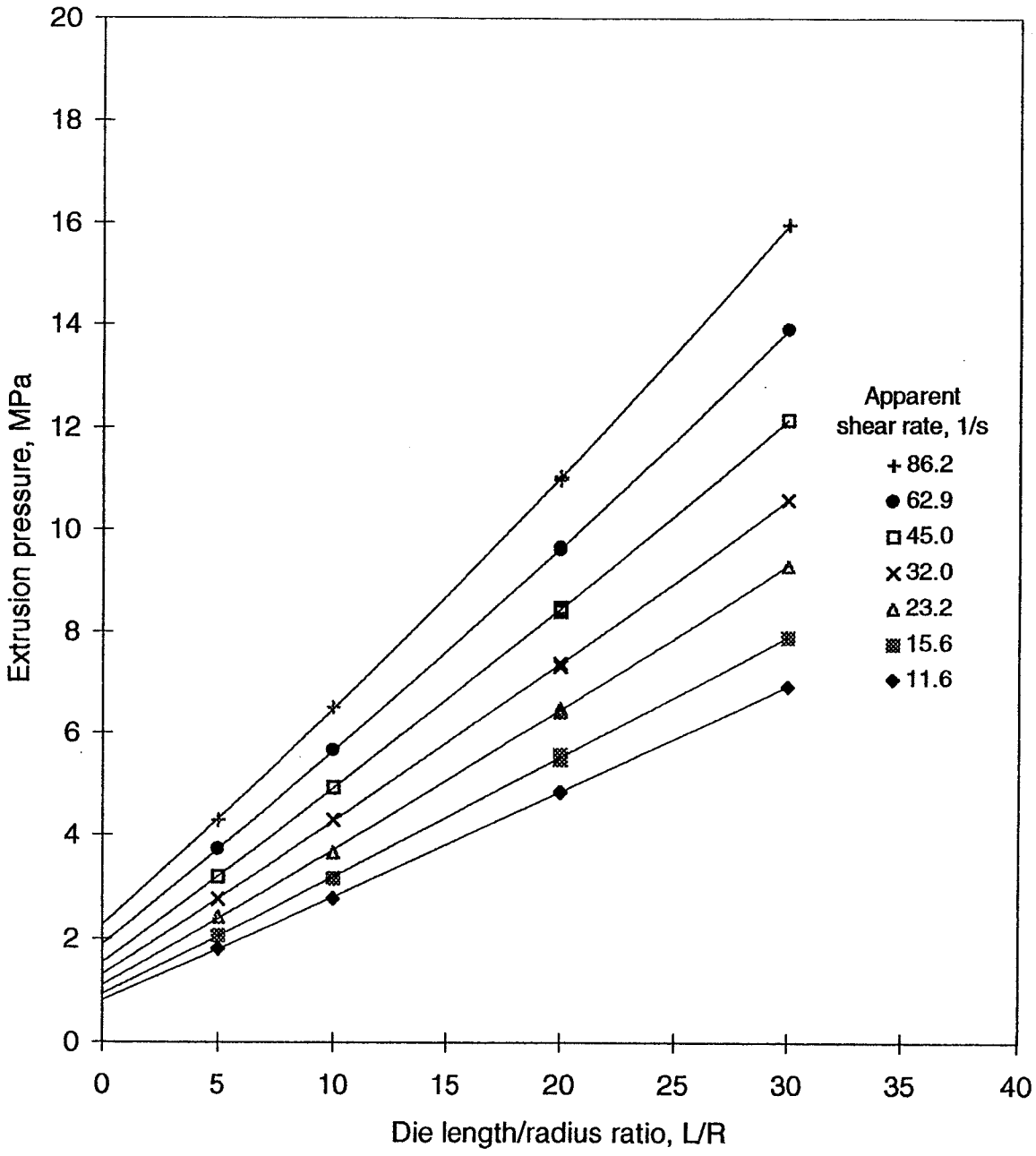

Figure 5: Bagley plot presented in Figure 4 but with a best-fit second order polynomial to the data.

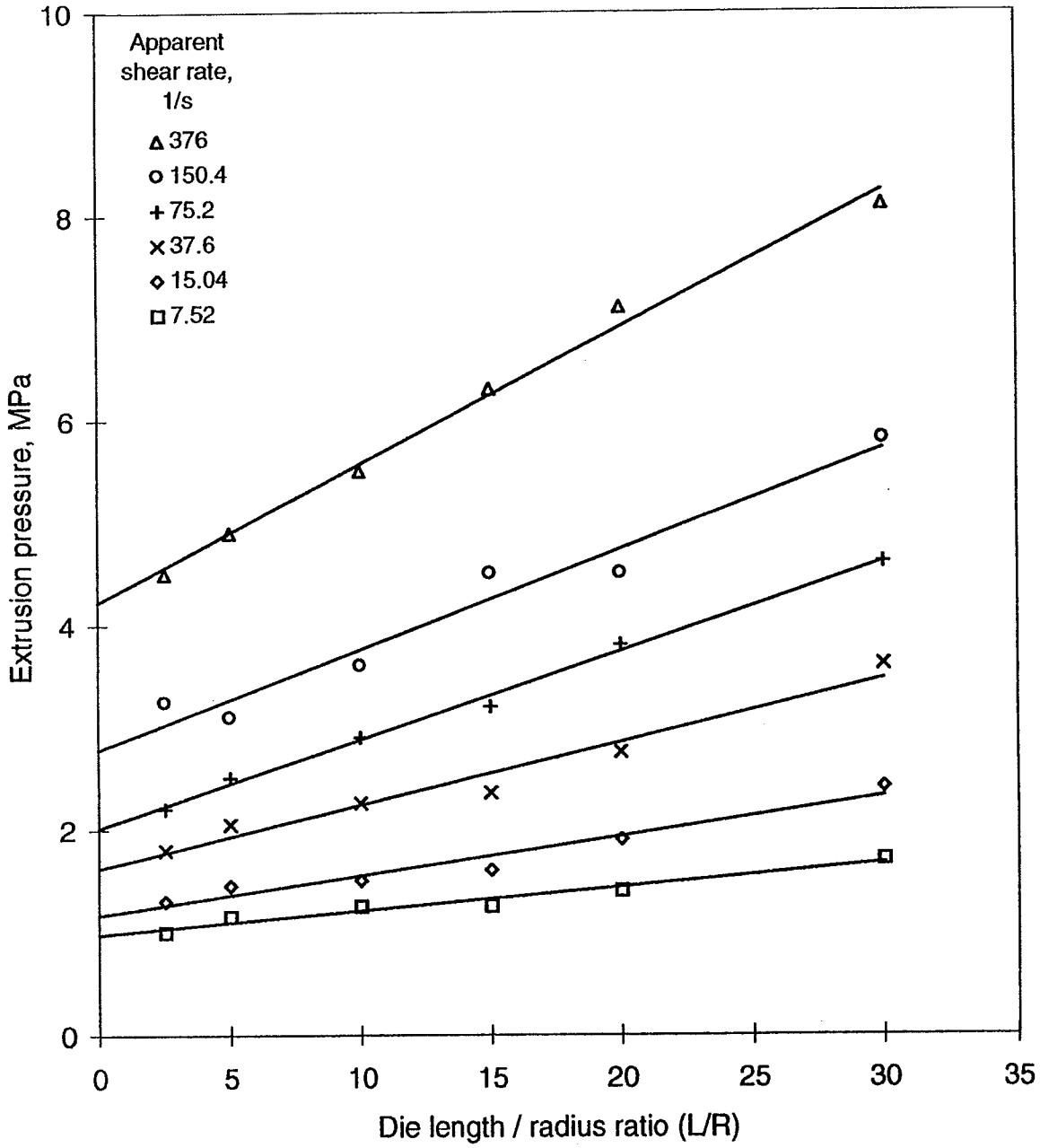

Figure 6: Bagley plot for an unsaturated polyester dough moulding compound containing 6 mm long glass fibres (DMC L7049) at 50 °C, exhibiting large entrance pressure drop values.

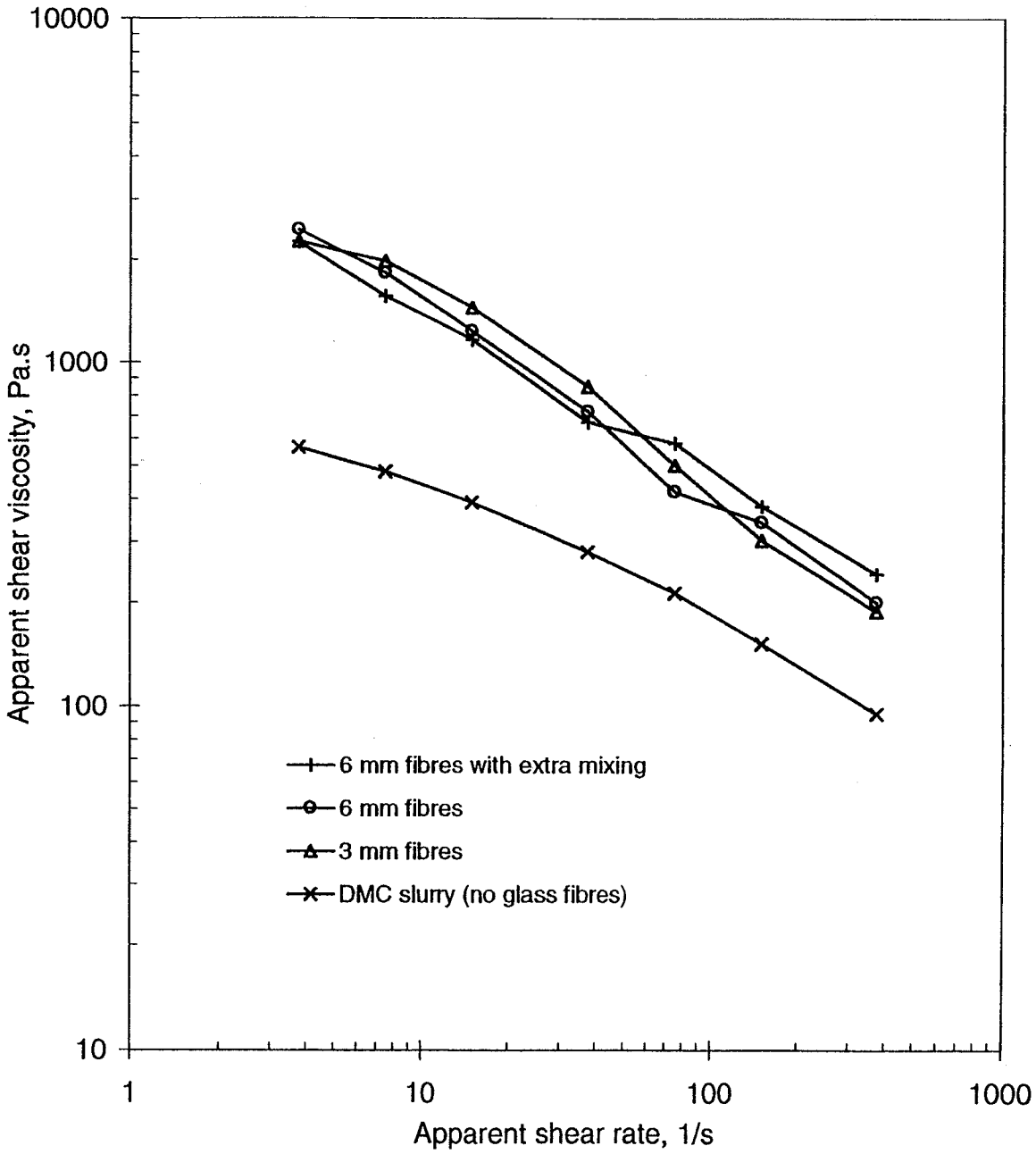

Figure 7: Effect of differences in glass fibre content on the shear viscosity of an unsaturated polyester dough moulding compound (DMC L7049) at 50 °C.

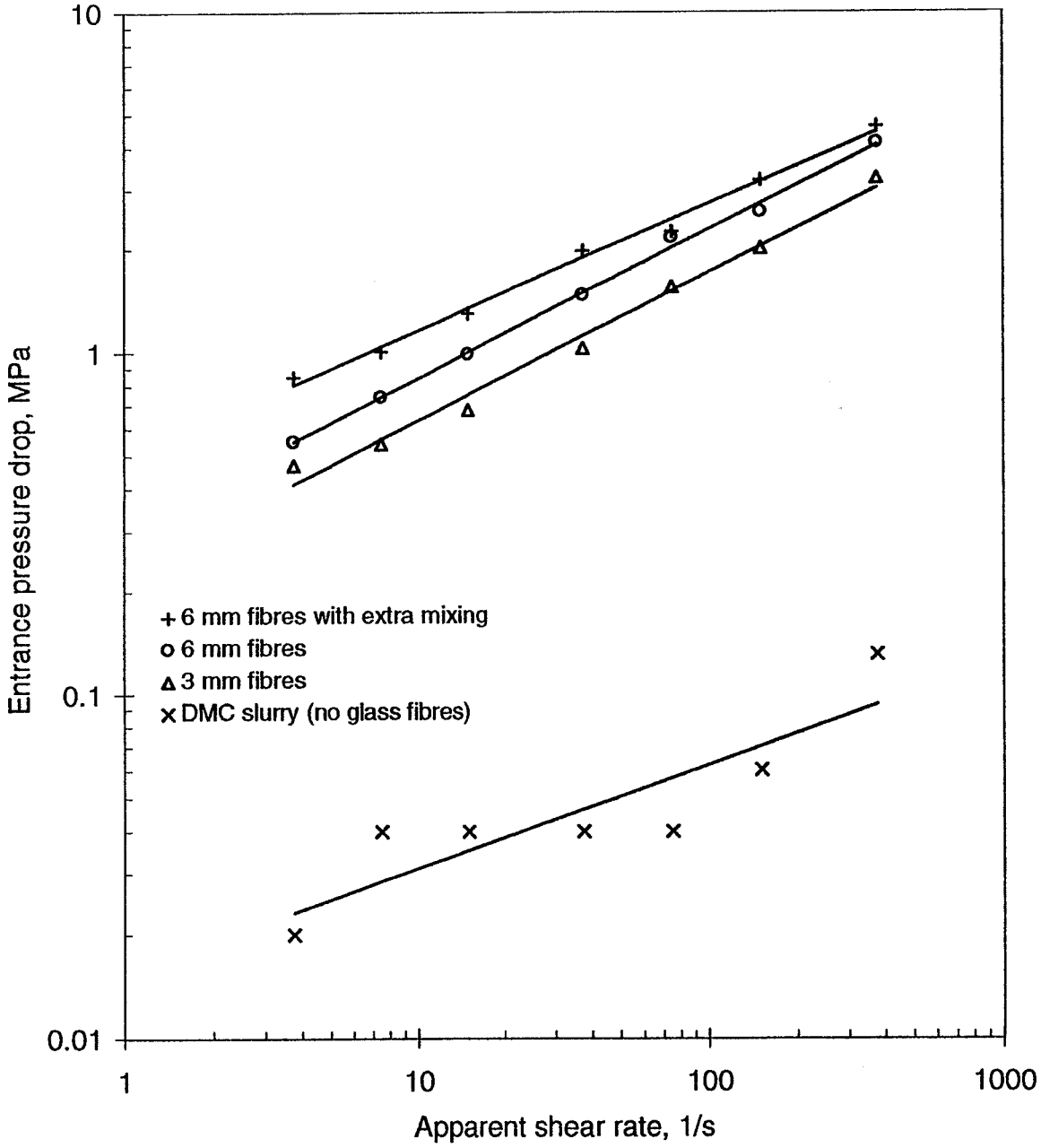

Figure 8: Effect of differences in glass fibre content on the entrance pressure drop values of an unsaturated polyester dough moulding compound (DMC L7049) at 50 °C.

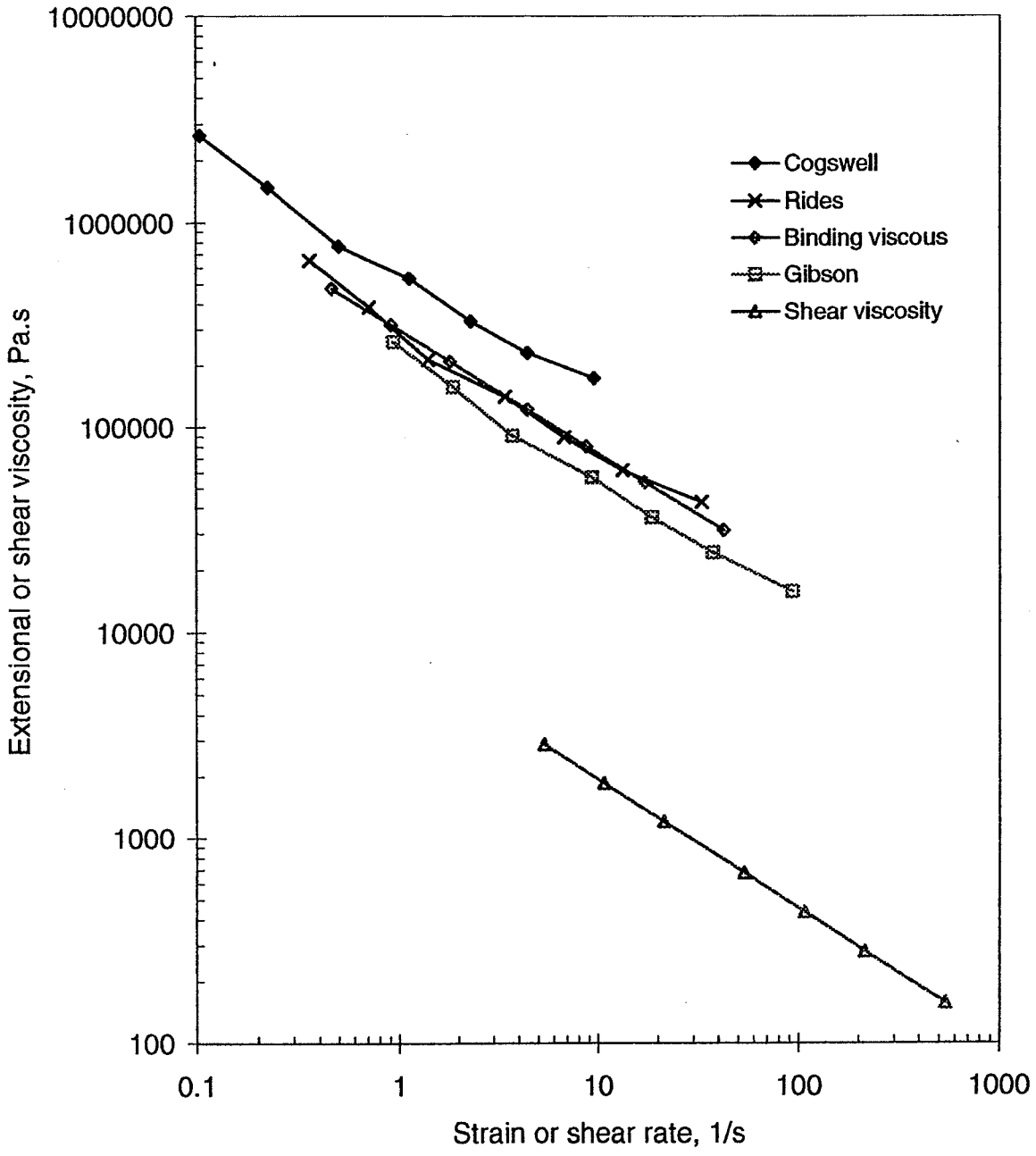

Figure 9: Comparison of predictions of the converging flow models for an unsaturated polyester dough moulding compound (DMC L7049) at 50 °C. Points on the Binding plot are for identification only rather than indicating actual data points.

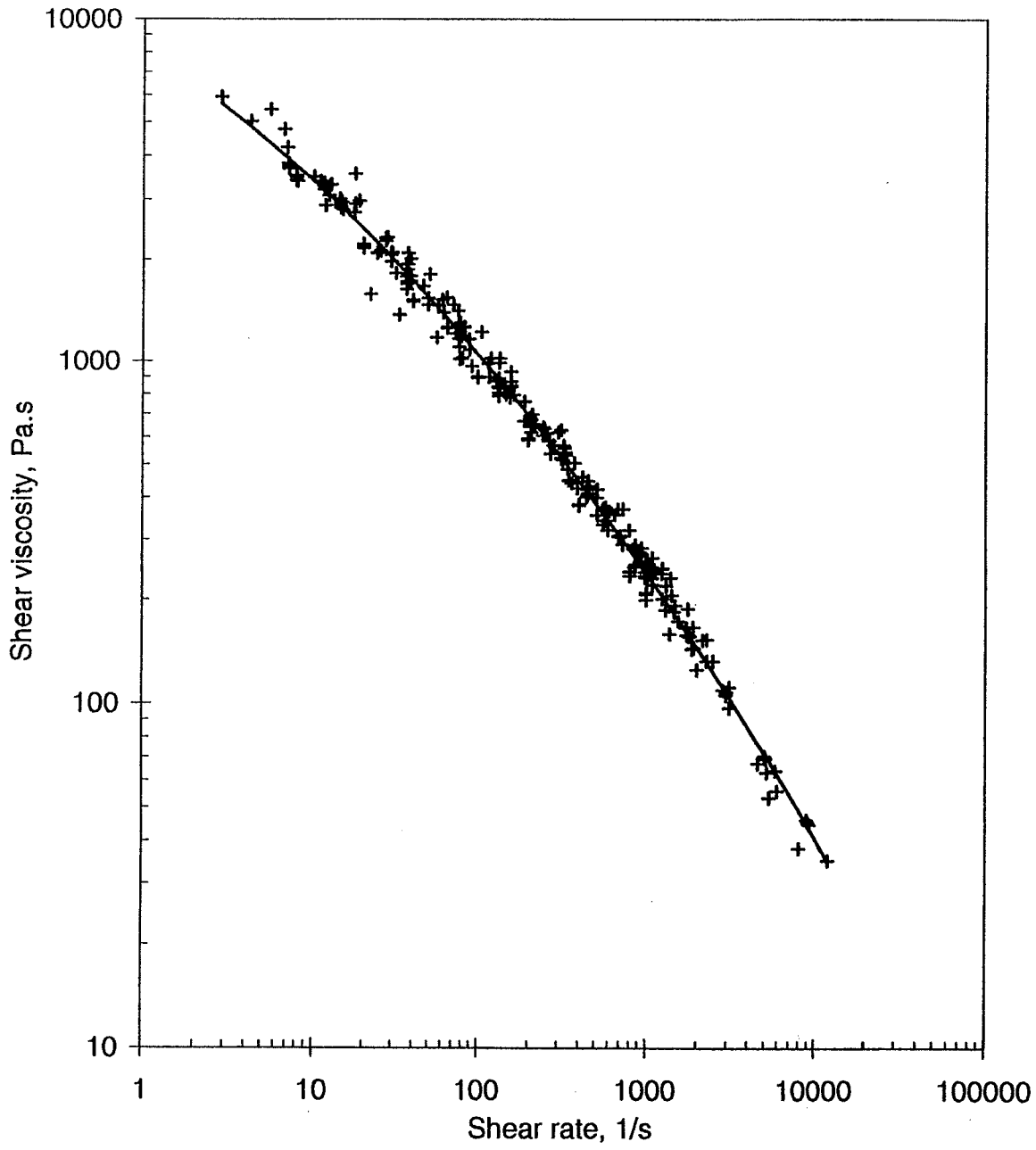

Figure 10: Scatter in shear viscosity values obtained for an HDPE (HFU000) at 190 °C in an intercomparison of capillary extrusion rheometry.

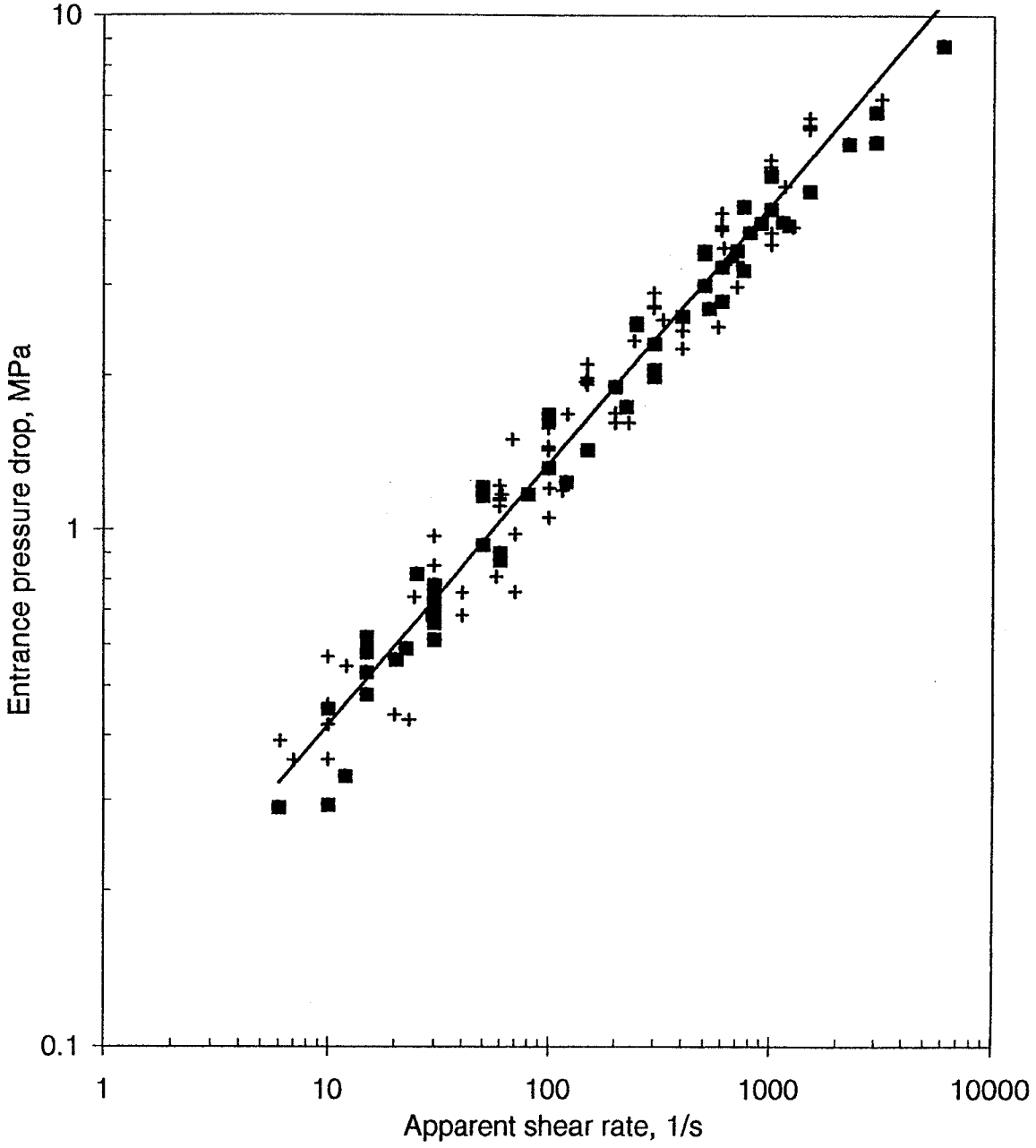

Figure 11: Scatter in entrance pressure drop values obtained for an HDPE (HFU000) at 190 °C in an intercomparison of capillary extrusion rheometry. Data obtained using barrel to die diameter contraction ratios in the range 9.55:1 - 15.5:1. Symbol ■ indicates data obtained using a contraction ratio of 15:1 only.

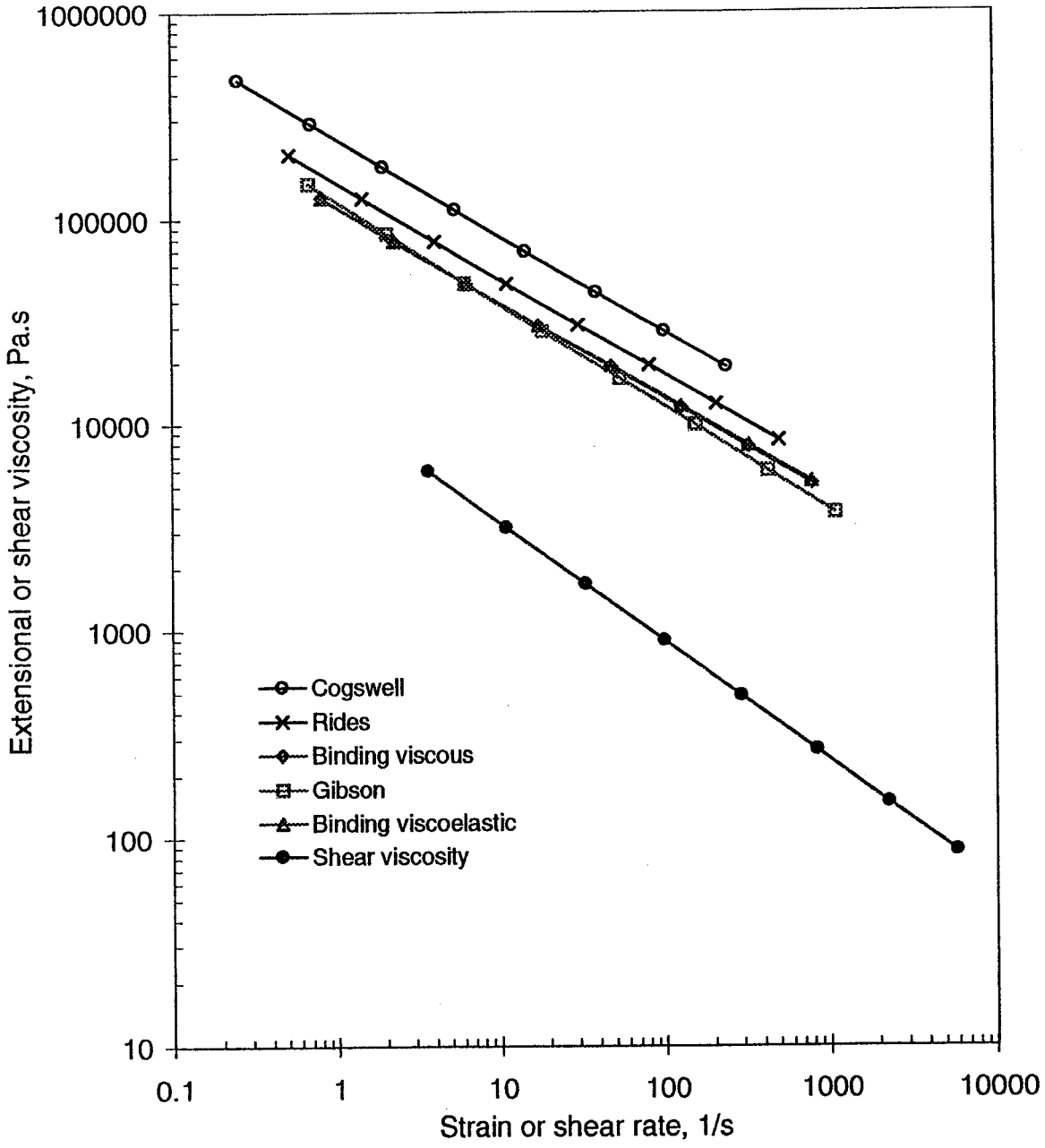

Figure 12: Comparison of predictions of the converging flow models for an HDPE (HFU000) at 190 °C. Points on the Binding plots are for identification only rather than indicating actual data points.

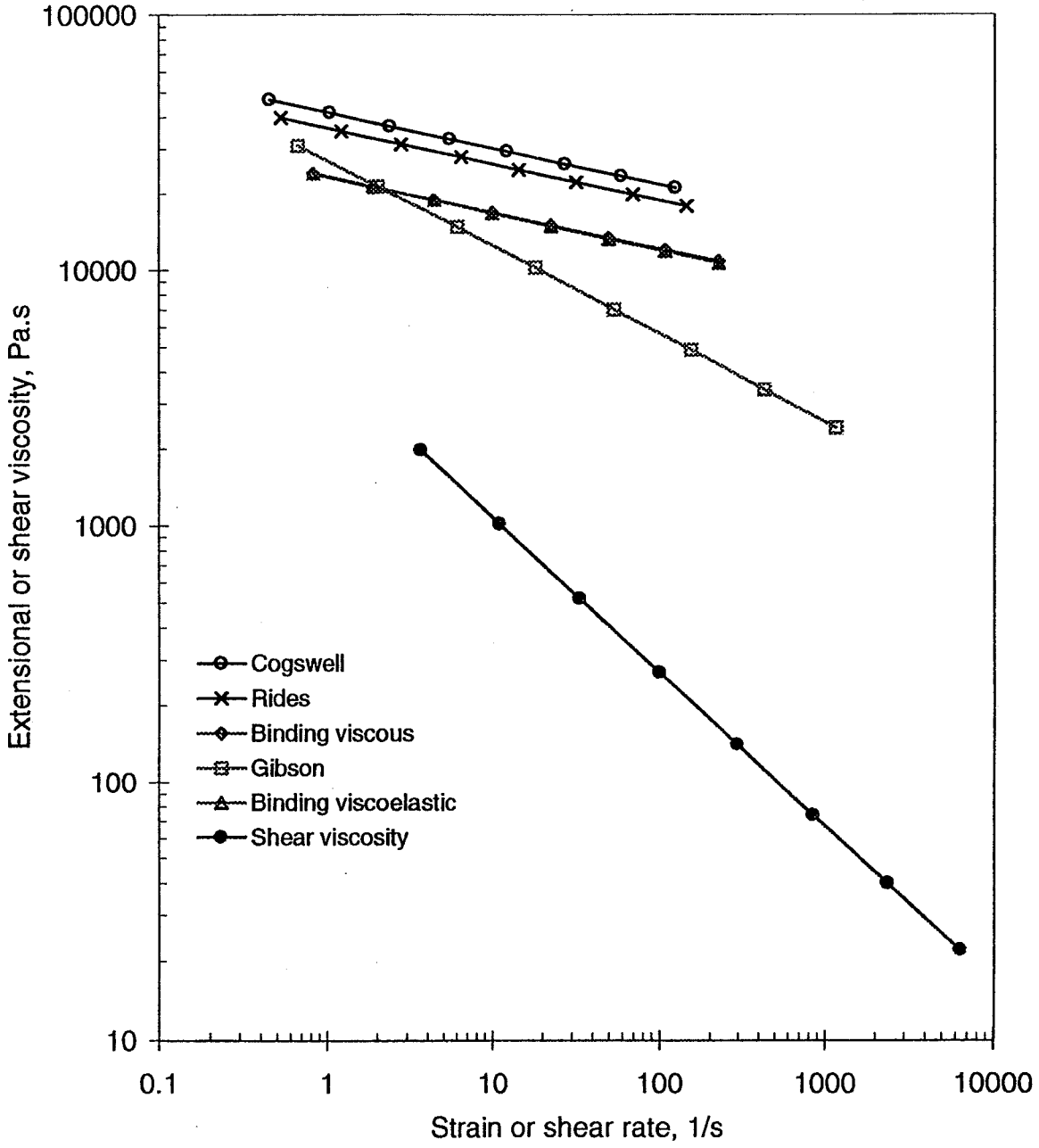

Figure 13: Comparison of predictions of the converging flow models for a glass fibre filled PP (HFQ000) at 230 °C. Points on the Binding plots are for identification only rather than indicating actual data points.

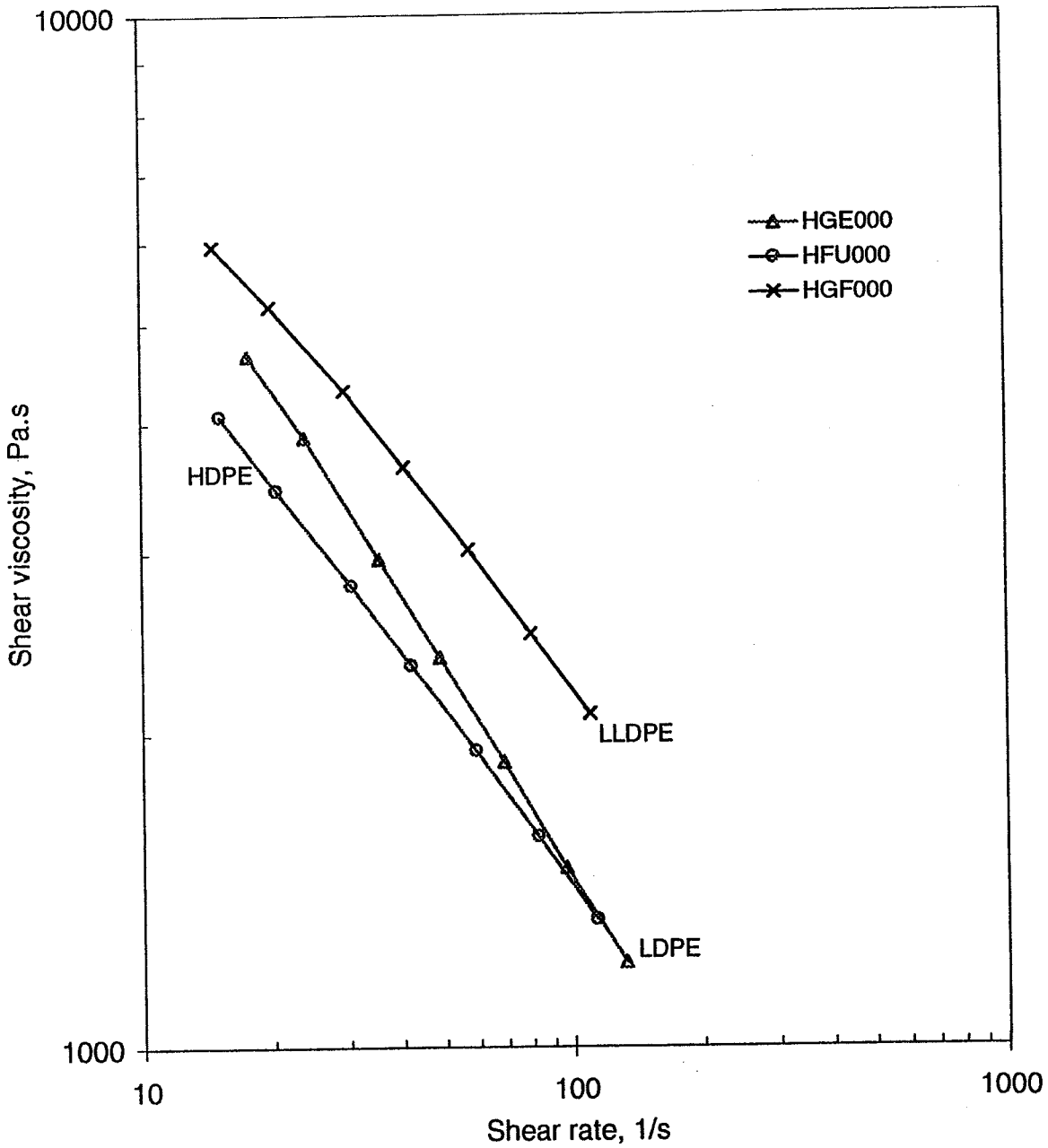

Figure 14: Comparison of shear viscosities of three polyethylenes LDPE (HGE000), LLDPE (HGF000) and HDPE (HFU000) at 150 °C.

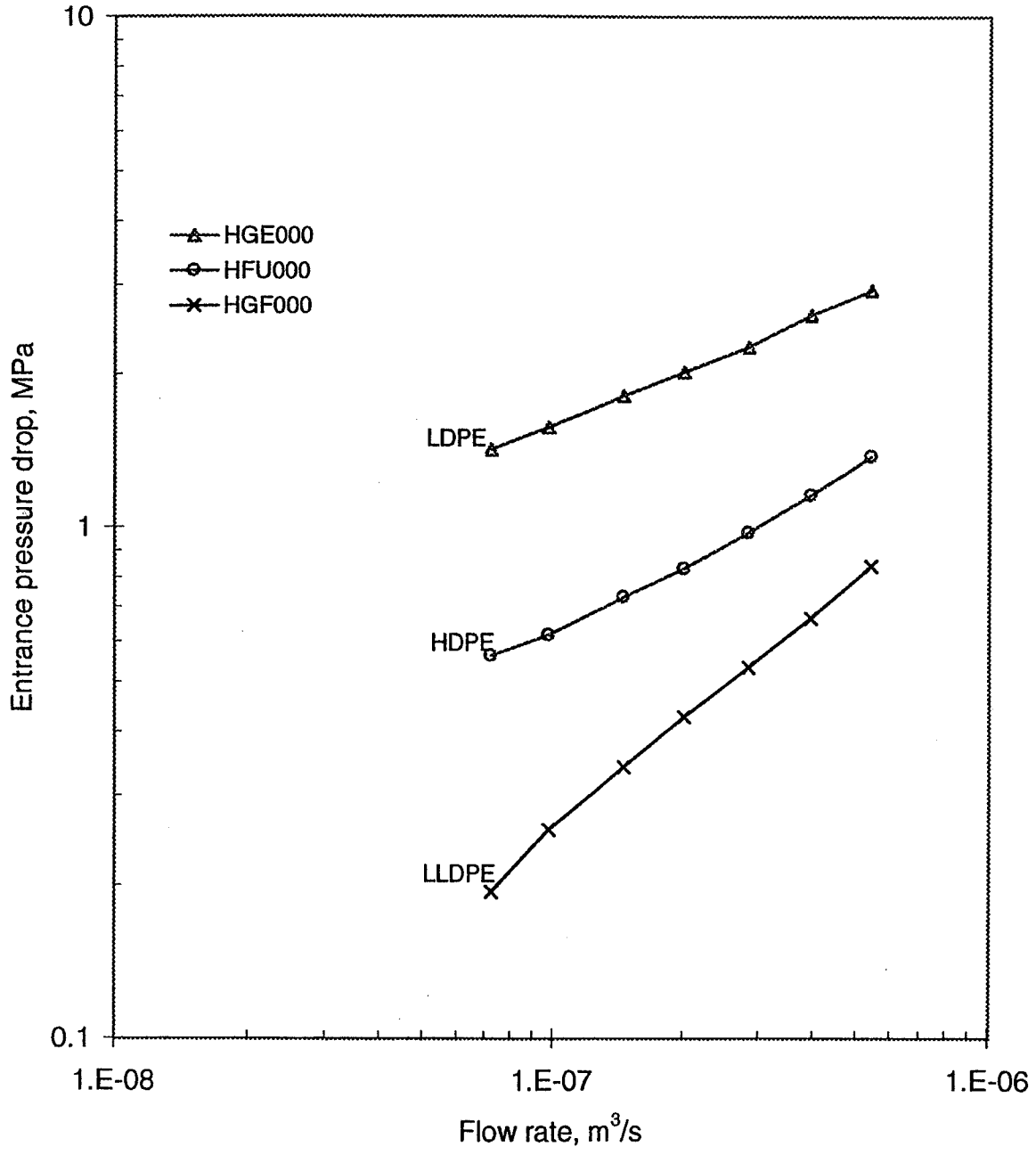

Figure 15: Comparison of entrance pressure drop values of three polyethylenes LDPE (HGE000), LLDPE (HGF000) and HDPE (HFU000) at 150 °C.

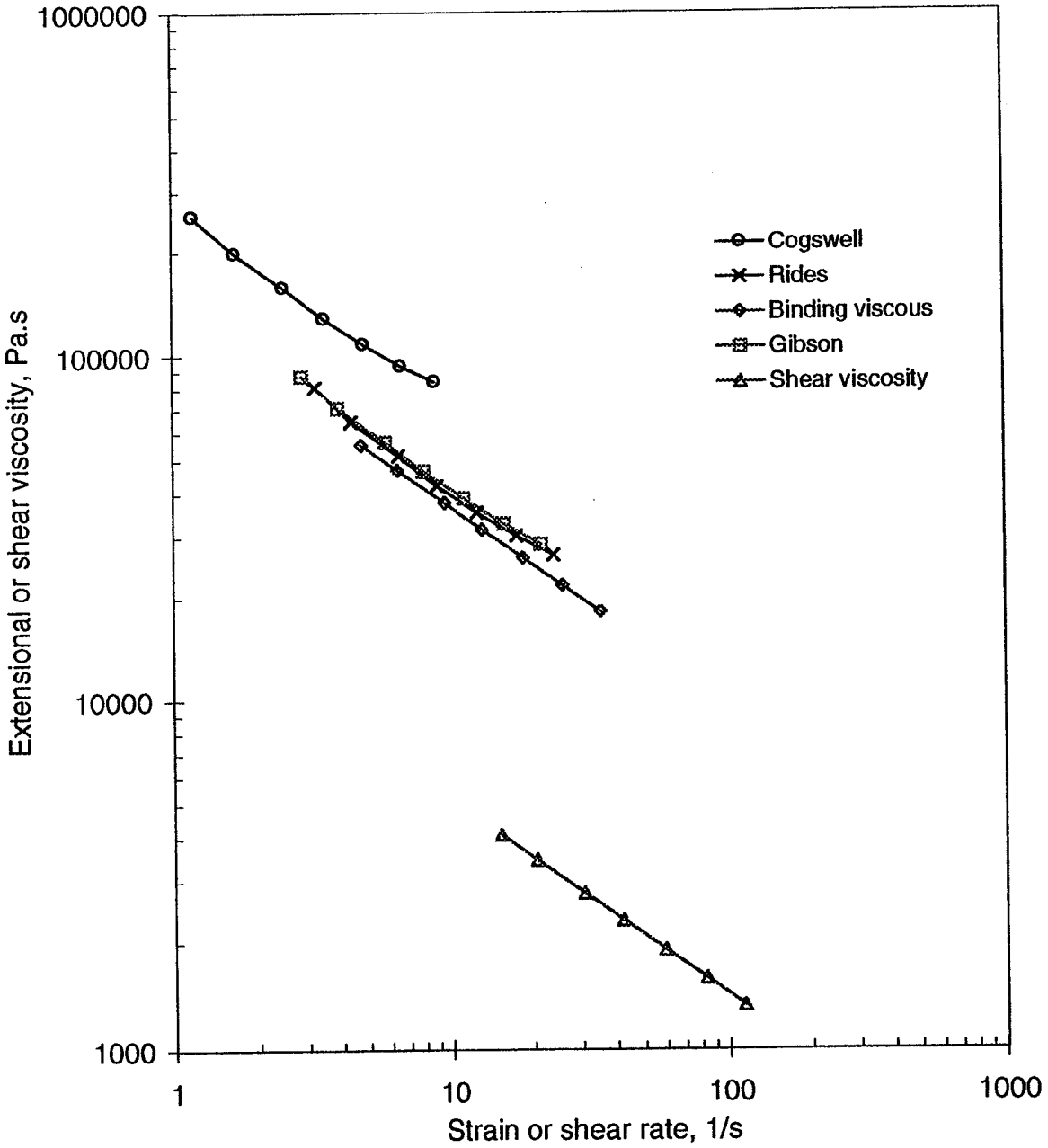

Figure 16: Comparison of predictions of the converging flow models for an HDPE (HFU000) at 150 °C. Points on the Binding plot are for identification only rather than indicating actual data points.

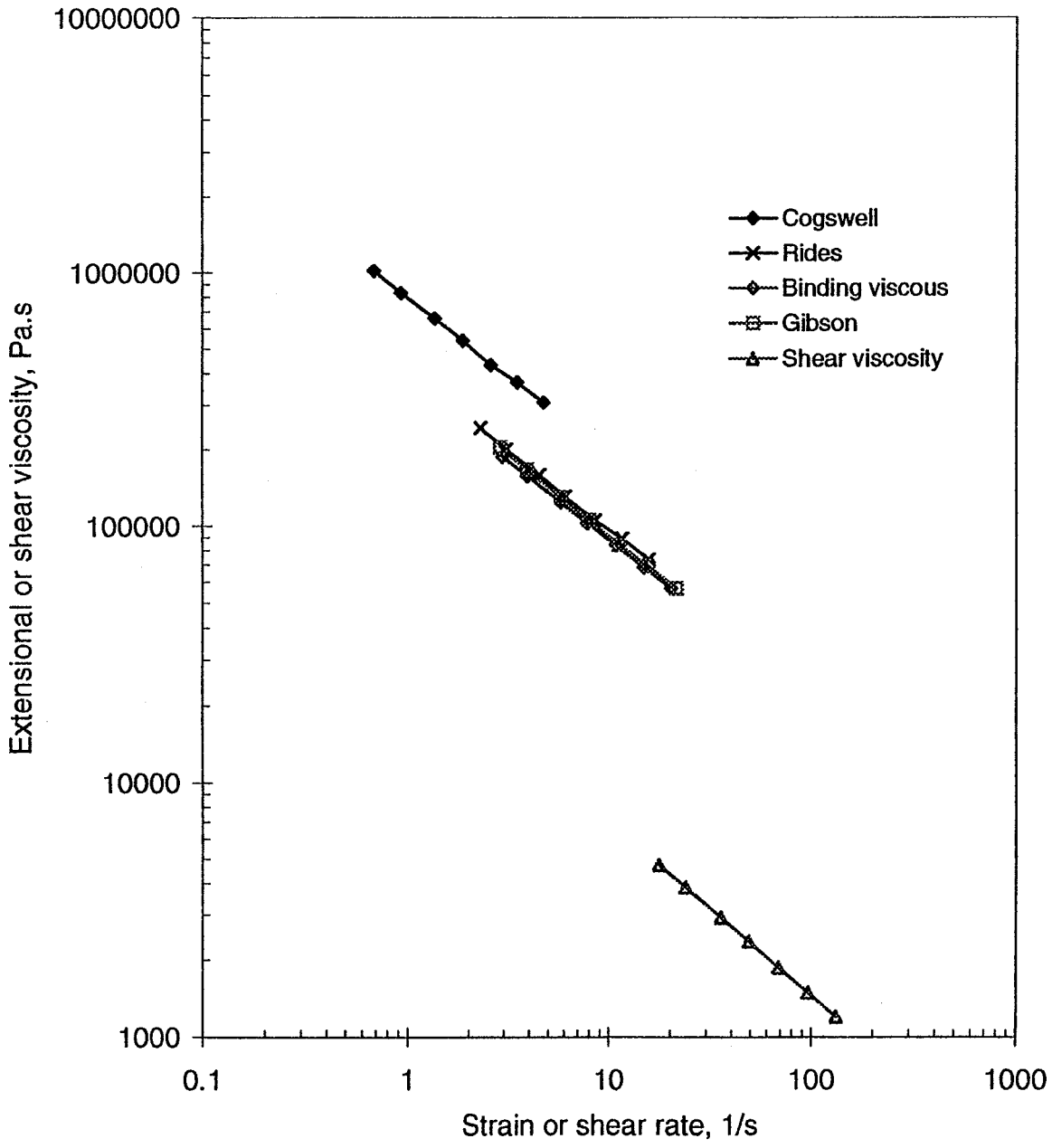

Figure 17: Comparison of predictions of the converging flow models for an LDPE (HGE000) at 150 °C. Points on the Binding plot are for identification only rather than indicating actual data points.

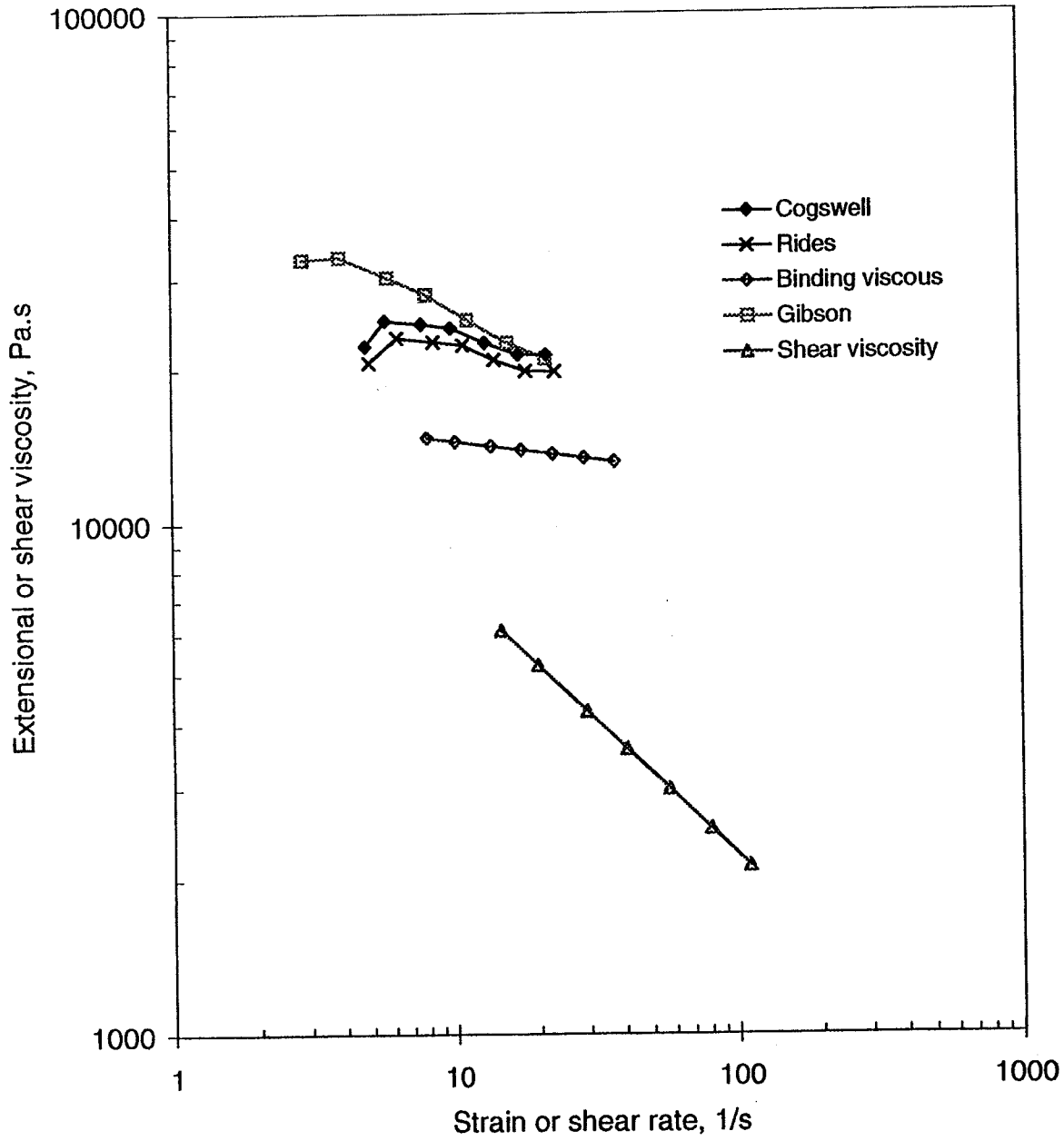

Figure 18: Comparison of predictions of the converging flow models for an LLDPE (HGF000) at 150 °C. Points on the Binding plot are for identification only rather than indicating actual data points.

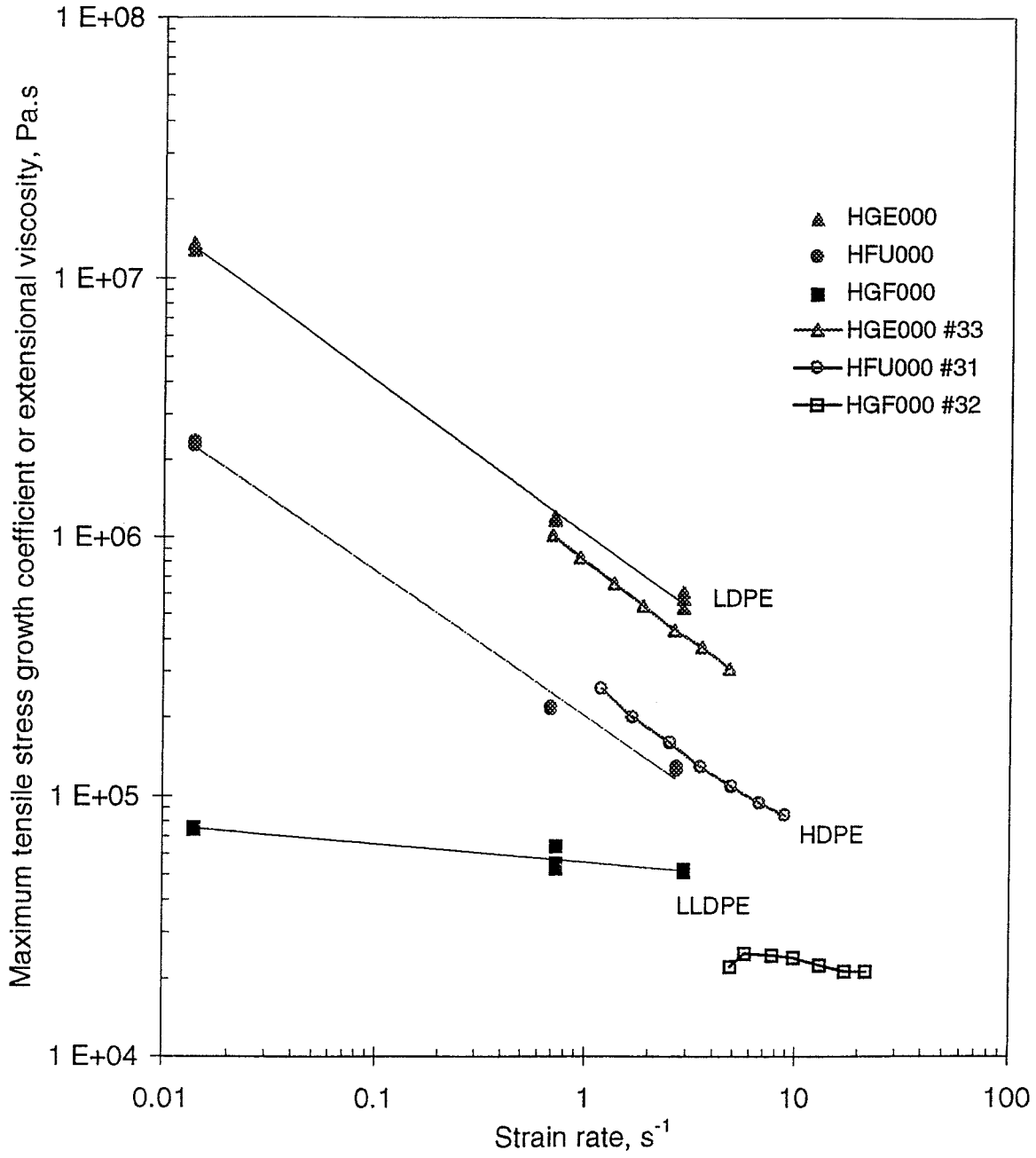

Figure 19: Comparison of extensional viscosities determined using the Cogswell converging flow model (open points) with maximum extensional stress growth coefficient values obtained by a stretching method (solid points) for three polyethylenes LDPE (HGE000), LLDPE (HGF000) and HDPE (HFU000) at 150 °C.

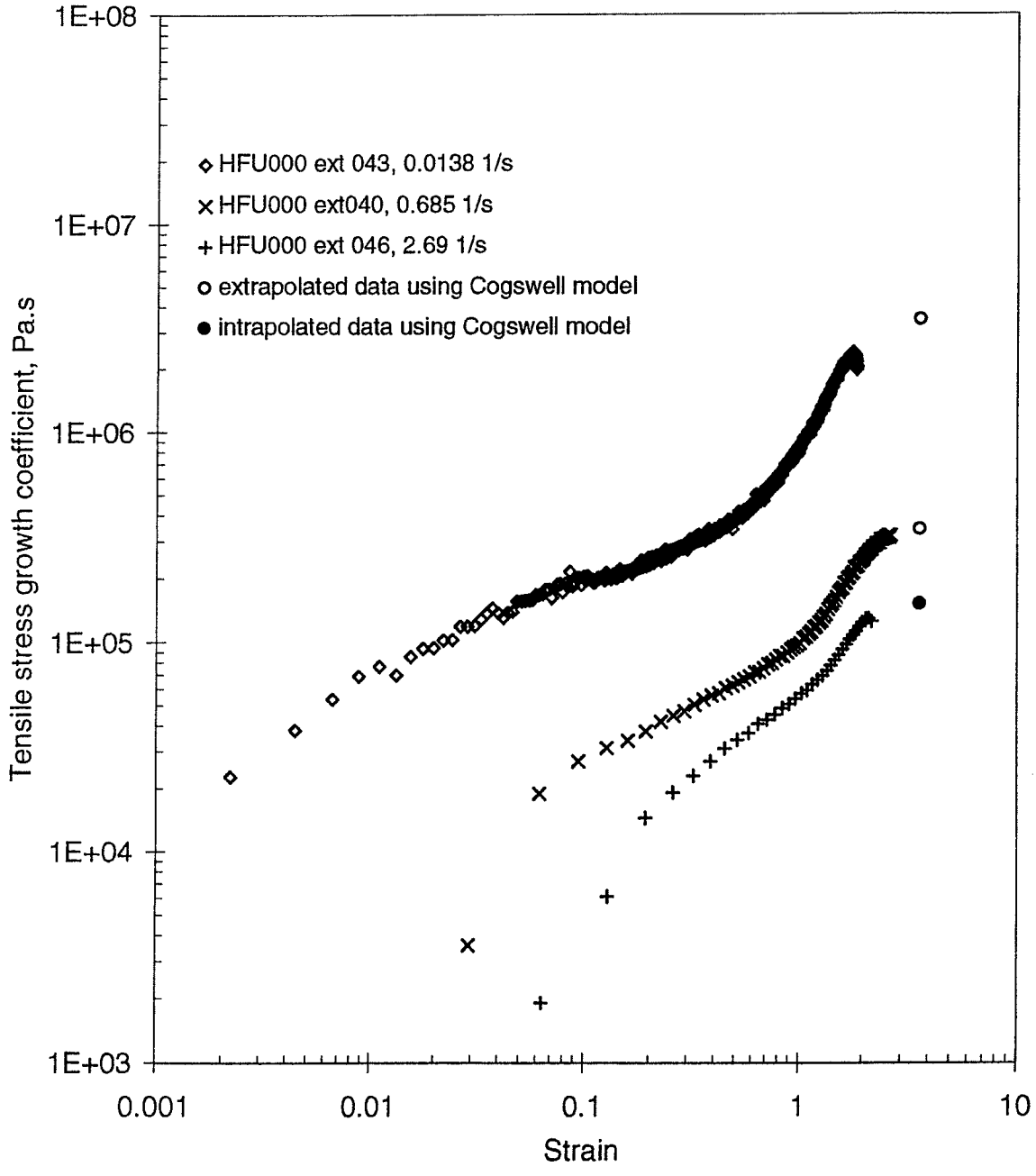

Figure 20: Comparison of extensional viscosities determined using the Cogswell converging flow model with extensional stress growth coefficient values obtained by a stretching method for HDPE (HFU000) at 150 °C.

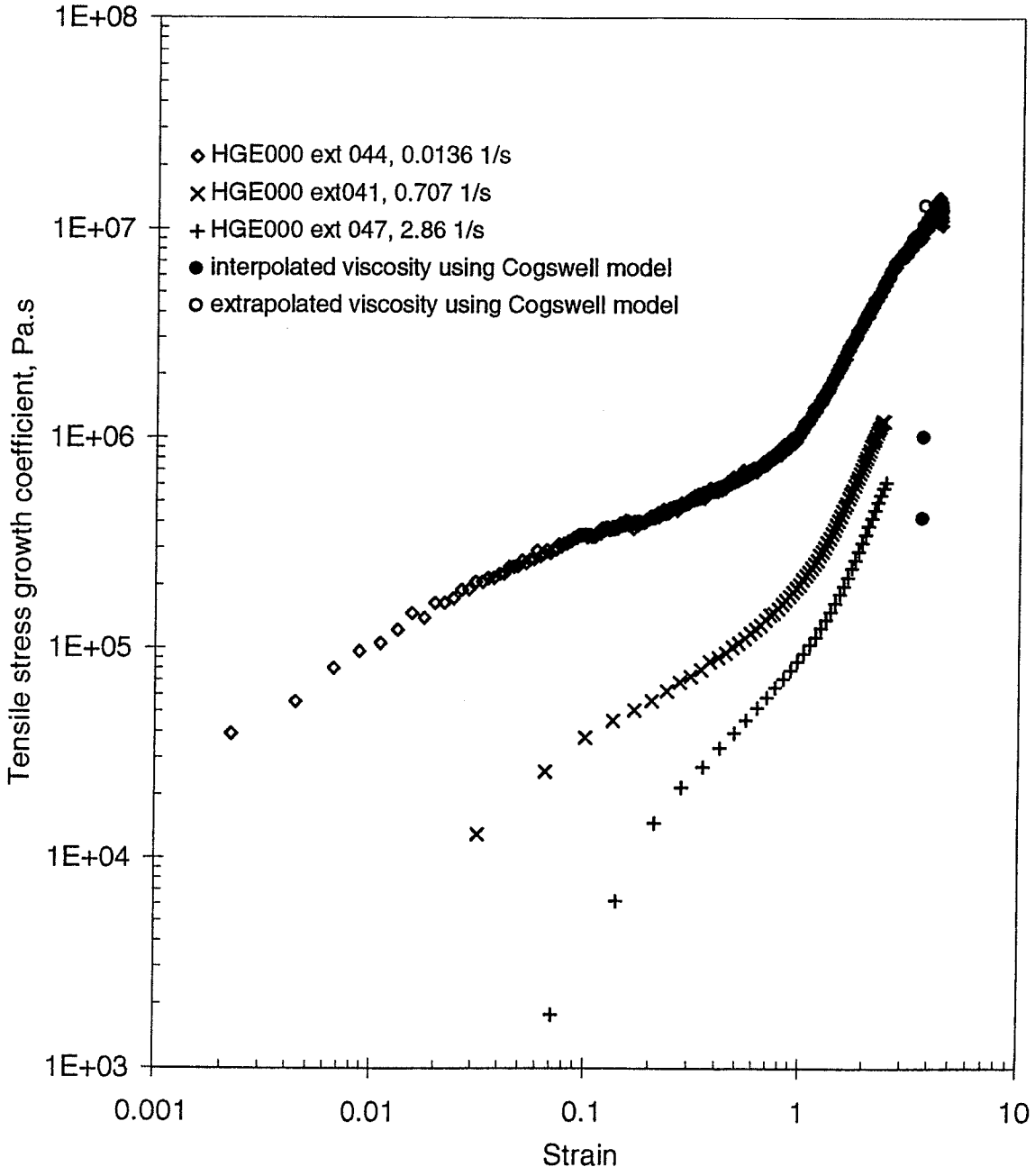

Figure 21: Comparison of extensional viscosities determined using the Cogswell converging flow model with extensional stress growth coefficient values obtained by a stretching method for LDPE (HGE000) at 150 °C.

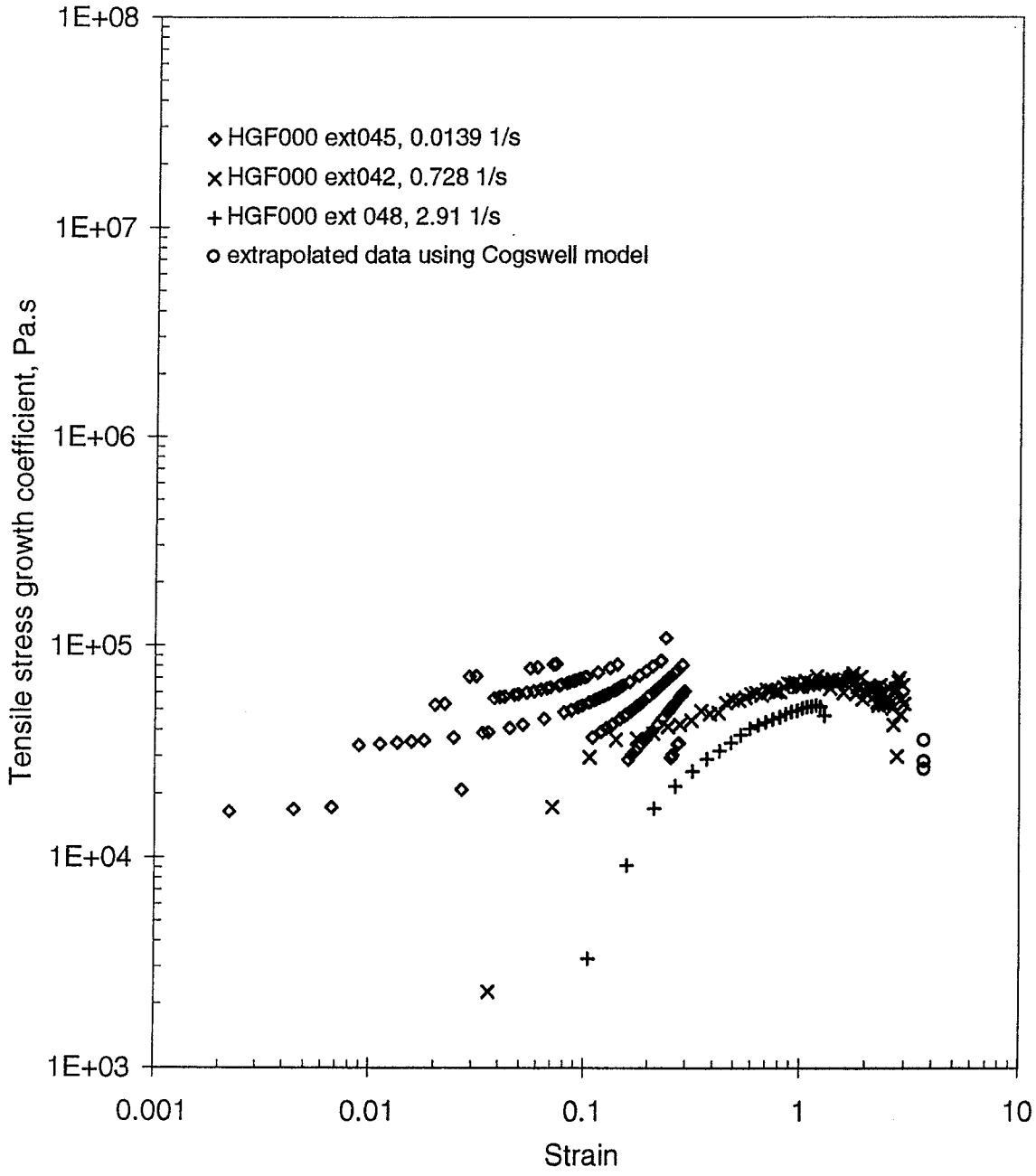

Figure 22: Comparison of extensional viscosities determined using the Cogswell converging flow model with extensional stress growth coefficient values obtained by a stretching method for LLDPE (HGF000) at 150 °C.

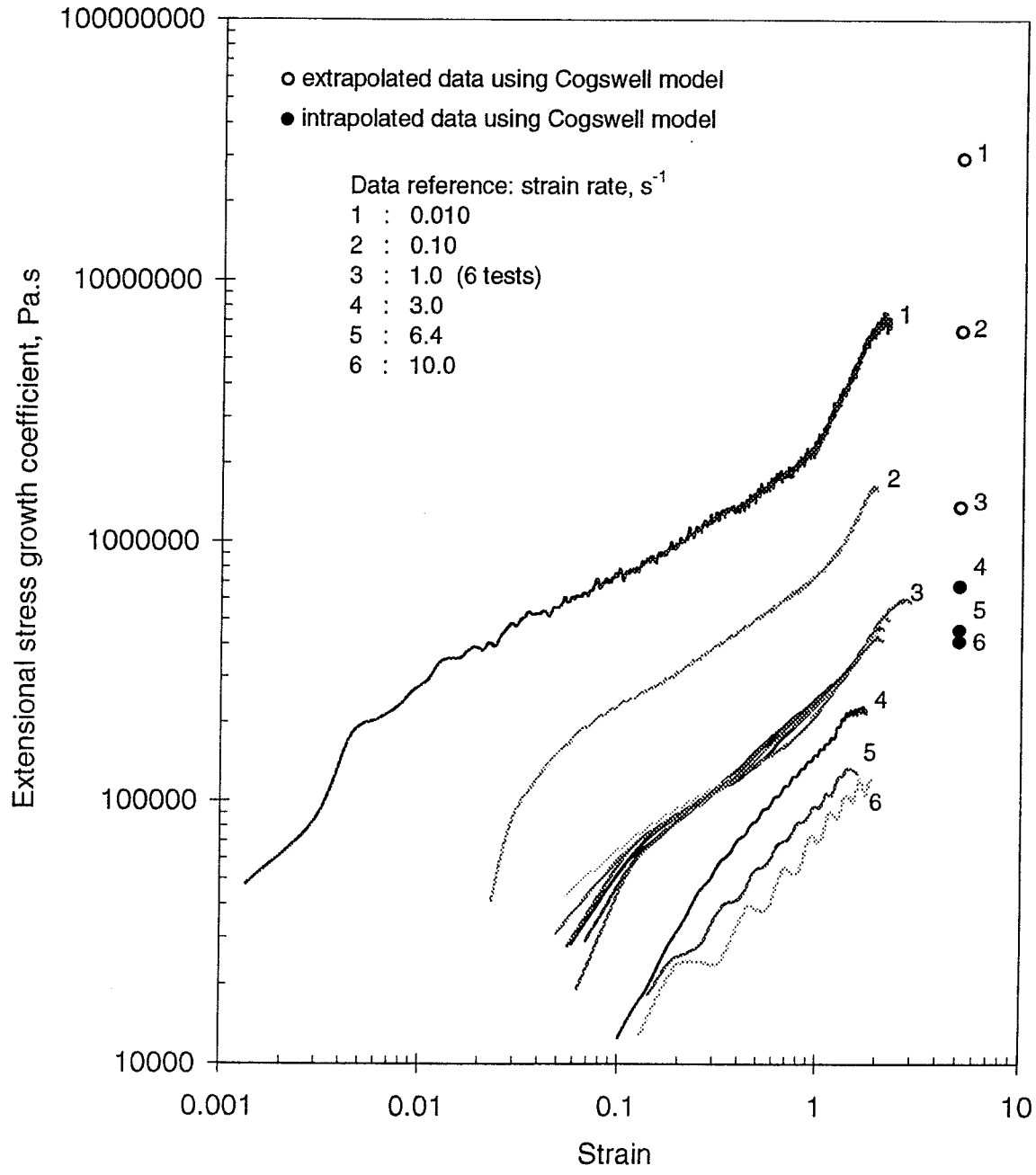

Figure 23: Comparison of extensional viscosities determined using the Cogswell converging flow model with extensional stress growth coefficient values obtained by a stretching method for HDPE (HGH000) at 150 °C.

Appendix A1: Definitions of strain, strain rate, stress and material properties functions in tensile (simple) extension

The following definitions are given by Whorlow (28) for strains and strain rates. Further descriptions are given by, for example, Gupta *et al* (29) and Dealy (30, 31).

A1.1 Elongation ratio

The *Elongation ratio (ER)* is the ratio of the current length ℓ to the initial length ℓ_o of the specimen:

$$ER = \ell / \ell_o. \qquad \text{(A1.1)}$$

A1.2 Cauchy ε_C and Hencky ε strains

The *Cauchy strain* ε_C is given by the ratio of the change in length $\delta\ell$ to the initial length ℓ_o of the specimen:

$$\varepsilon_C = \delta\ell / \ell_o. \qquad \text{(A1.2)}$$

The *Hencky strain* ε (also referred to as the natural or true strain) is given by the natural logarithm of the elongation ratio:

$$\varepsilon = \ln(\ell / \ell_o) \qquad \text{(A1.3)}$$

Thus the elongation ratio is related to the Cauchy strain by

$$ER = 1 + \varepsilon_C \qquad \text{(A1.4)}$$

$$\text{i.e.} \quad \ell / \ell_o = 1 + \delta\ell / \ell_o. \qquad \text{(A1.5)}$$

To illustrate the difference between these measures of strain a specimen that was stretched to 10 times its original length has an elongation ratio of 10, a Cauchy strain of 9 and a Hencky strain of 2.3.

A1.3 Cauchy $\dot{\varepsilon}_c$ and Hencky $\dot{\varepsilon}$ strain rates

The *Cauchy strain rate* is given by

$$\dot{\varepsilon}_c = 1/\ell_o \times \partial\ell/\partial t \qquad \text{(A1.6)}$$

and the *Hencky strain rate* by

$$\dot{\varepsilon} = 1/\ell \times \partial\ell/\partial t \qquad \text{(A1.7)}$$

In describing and modelling plastics processing the Hencky strain is preferred as the rate of strain of an element of fluid within the flow is independent of its original length and is determined only from the velocity field of that element. It is thus a more suitable characteristic of the flow.

A1.4 Extensional flows: velocity fields

Terminology and definitions for materials functions describing the response of viscoelastic fluids to various shearing and extensional deformations are presented by Dealy (32). Mathematical descriptions of extensional flows were presented, for example, by Meissner et al (33) and Walters (34).

For *tensile (simple or uniaxial) extension* where $\dot{\varepsilon}$ is the true strain rate and ε is the true strain, defined as

$$\varepsilon = \ln(\ell/\ell_o) \qquad \text{(A1.8)}$$

then in rectangular coordinates:

$$v_1 = \dot{\varepsilon}\, x_1 \qquad \text{(A1.9)}$$

$$v_2 = -\tfrac{1}{2}\,\dot{\varepsilon}\, x_2 \qquad \text{(A1.10)}$$

$$v_3 = -\tfrac{1}{2}\,\dot{\varepsilon}\, x_3 \qquad \text{(A1.11)}$$

where $\dot{\varepsilon} \geq 0$.

Alternatively, in cylindrical coordinates:

$$v_z = \dot{\varepsilon}\, z \qquad \text{(A1.12)}$$

$$v_r = -\tfrac{1}{2}\, \dot{\varepsilon}\, r \qquad \text{(A1.13)}$$

where $\dot{\varepsilon} \geq 0$.

A1.5 Material properties

Following the notation presented by Dealy (32) and prepared by the Nomenclature Committee of the Society of Rheology, for start-up flow in tensile (simple) extension at constant (Hencky) strain rate $\dot{\varepsilon}$ the following definitions are given. Equivalent expressions for cessation of steady tensile extension, tensile creep, tensile recoil and tensile step strain are presented by Dealy (32).

A1.5.1: Net tensile stress

The *net tensile stress* σ_E is defined by

$$\sigma_E = \sigma_{11} - \sigma_{22} = \sigma_{11} - \sigma_{33} = \sigma_{zz} - \sigma_{rr} \qquad \text{(A1.14)}$$

where σ_{ij} is a stress tensor in either rectangular or axisymmetric co-ordinates. The tensile stress growth function is indicated by σ_E^+ where the + indicates start-up rather than cessation of flow.

A1.5.2 Tensile stress growth coefficient

The *tensile stress growth coefficient* η_E^+ is defined by:

$$\eta_E^+(t, \dot{\varepsilon}) = \sigma_E / \dot{\varepsilon} \qquad \text{(A1.15)}$$

where t is time.

A1.5.3 Tensile viscosity

The *tensile viscosity* η_E is defined by:

$$\eta_E(t, \dot{\varepsilon}) = \lim_{t \to \infty} [\eta_E^+(t, \dot{\varepsilon})] \qquad \text{(A1.16)}$$

It defines the limiting extensional viscosity and as such represents an equilibrium extensional viscosity if a steady value is achieved.

Appendix A2: Uncertainties in the determination of entrance pressure drop values

In determining entrance pressure drop values it is desirable to follow a procedure that minimises the errors and uncertainty in the values determined. The uncertainty in entrance pressure drop values stems principally from the measurement of the extrusion pressure at each flow rate and for each die. As described in Section 6.3 at least two dies of different length but of the same diameter and entry geometry are necessary to determine shear viscosity and entrance pressured drop values. Short or "zero" length dies - die of the order of 1 mm or less in length - have been used to measure the entrance pressure drop directly. A second long die is then needed in order to determine the shear viscosity. To assess the uncertainty in the determination of entrance pressure drop values using either the Bagley method or by direct measurement using a short die, the following uncertainty analysis is derived. Analysis of the uncertainties in the measurement of shear viscosity are presented elsewhere [26].

In referring to Figure 2 the gradient of the best-fit straight line to data obtained at an apparent shear rate $\dot{\gamma}_{ap1}$ can be expressed on the basis of the interval either from the origin to $(L/R)_1$, or from $(L/R)_1$ to $(L/R)_2$. As these terms are equivalent then

$$gradient = \frac{P_1 - P_{ent1}}{(L/R)_1} = \frac{P_2 - P_1}{(L/R)_2 - (L/R)_1} \qquad \text{(A2.1)}$$

This expression can be rewritten as

$$P_{ent} = P_1 - \frac{(P_2 - P_1) \times (L/R)_1}{(L/R)_2 - (L/R)_1} \qquad \text{(A2.2)}$$

or

$$P_{ent} = P_1 - (P_2 - P_1)A \qquad \text{(A2.3)}$$

or

$$P_{ent} = P_1 + P_1 A - P_2 A \qquad \text{(A2.4)}$$

where

$$A = \frac{(L/R)_1}{(L/R)_2 - (L/R)_1} \qquad \text{(A2.5)}$$

Assuming that the value of the term A can be accurately determined, i.e. the uncertainty associated with the measurement of the die length and diameter is negligible, then the fractional uncertainty in the entrance pressure drop p_{ent}/P_{ent} can then be written as

$$\left(\frac{p_{ent}}{P_{ent}}\right)^2 = \frac{(p_1)^2 + (p_1 A)^2 + (p_2 A)^2}{\left(P_1 + P_1 A - P_2 A\right)^2} \qquad \text{(A2.6)}$$

where the use of the lower case indicates the uncertainty in the parameter, and the upper case indicates the value of the parameter. The ratio of the uncertainty in the parameter to the value of the parameter is the fractional uncertainty of that parameter. Substitution of appropriate values into Equation A2.6 thus yields a fractional uncertainty value for the entrance pressure drop.

To illustrate this analysis the case of the data obtained for an HDPE at 190 °C, Figure 4, is now used to assess the uncertainty in the derived entrance pressure drop values. The following approximate values were determined from Figure 4 for the highest apparent shear rate data.

P_1 = 4 MPa, $(L/R)_1$ = 5
P_2 = 16 MPa, $(L/R)_2$ = 30

Thus the term A = 0.2. Assuming that the uncertainties in P_1 and P_2 are both 0.05 MPa - estimated from the variation in data obtained from repeat testing using the die L/R = 20 - then the fractional uncertainty in the entrance pressure drop value determined using the Bagley method is calculated as ≈ 3%.

In using this method the entrance pressure drop can be estimated using

$$P_{ent} = \left(P_1 + P_1 A - P_2 A\right) \qquad \text{(A2.7)}$$

Thus the error in using a short die and assuming that the entrance pressure drop is equivalent to the extrusion pressure drop for that die can also be assessed, and is given by

$$\%\ \text{error in using } P_1 \equiv P_{ent} = 100\% \times \left(\frac{P_2 A - P_1 A}{P_1 + P_1 A - P_2 A}\right) \qquad \text{(A2.8)}$$

The fractional uncertainty in the measurement of pressure using the short die is given simply by p_1/P_1.

Further results for the above case and other cases involving variations in the flow rate and die length are presented in Table 1.

It is noted from Table 1 that using a short die of 1 mm length and assuming that the extrusion pressure obtained using it is equivalent to the entrance pressure drop may result in a smaller uncertainty in the entrance pressure drop value (2.4% c.f. 3.1% for the Bagley method) but that in so doing the entrance pressure is in error by $\approx$ 30% compared with that obtained by extrapolation. In using a 0.1 mm length die this error is still $\approx$ 3% - 4%.

Appendix A3: Cogswell converging flow models: free and constrained convergence

For reasons of consistency the notation used in this Appendix is not necessarily the same as that used in the original reference [7].

The converging flow model developed by Cogswell (7) has two versions; one is applicable to the analysis of freely converging flow and the other to constricted converging flow. Free convergence occurs when the flow establishes its own primary-secondary flow boundary or vortex within the confines of the contraction region, see Figure 1 (primary refers to the main flow through the die and secondary refers to any vortex or stagnant region formed in the die entry region). Constricted converging flow occurs when no secondary flow region is formed, such as when using an entry cone of angle less than that of the naturally occurring primary-secondary flow boundary. Both cases are considered below.

In the converging flow model it was assumed that apparent shear viscosity η_{ap} was described by the power-law behaviour

$$\eta_{ap} = \eta_{o,ap} \dot{\gamma}_{ap}^{\,n-1} \qquad \text{(A3.1)}$$

and extensional viscosity λ was independent of strain rate

$$\lambda = \lambda_o \qquad \text{(A3.2)}$$

where $\eta_{o,ap}$, n and λ_o are constant for a given temperature and the apparent shear rate $\dot{\gamma}_{ap}$ is given by

$$\dot{\gamma}_{ap} = \frac{4Q}{\pi R_o^{\,3}} \qquad \text{(A3.3)}$$

The analysis considered that the converging flow region was comprised of a series of short truncated conical elements of decreasing diameter. The velocity profile of the flow in each element was assumed to be the same as that for fully developed shear flow. The shear flow pressure drop for the element was determined by integration over the length of the tapered element. The extensional flow pressure drop was based on the average extension rate over the length of the element, and as such was independent of the assumed velocity profile. The shear flow pressure drop ΔP_S and the extensional flow pressure drop ΔP_E for a conical element of entry radius R_i, exit radius R_o ($R_o < R_i$) and converging angle α are given by

$$\Delta P_s = 2 \frac{\left(\eta_{ap}\big|_{r=Ro}\right)}{3n \tan\alpha} \left[\frac{4Q}{\pi R_o^3}\right] \left[1 - \left(\frac{R_o}{R_i}\right)^{3n}\right] \qquad \text{(A3.4)}$$

and

$$\Delta P_E = \frac{\lambda \tan\alpha}{3}\left[\frac{4Q}{\pi R_o^3}\right]\left[1 - \left(\frac{R_o}{R_i}\right)^3\right] \qquad \text{(A3.5)}$$

where $\eta_{app}|_{r=Ro}$ denotes the apparent shear viscosity evaluated for the apparent shear-rate for flow rate Q in a channel of radius R_o (Equations A3.1 and A3.7). The total pressure drop ΔP_{ent} for the element was calculated, assuming additivity, as the sum of the shear and extensional flow pressure drops. Thus

$$\Delta P_{ent} = \Delta P_s + \Delta P_E \qquad \text{(A3.6)}$$

For constricted converging flow the total pressure drop P_{ent} in an entry region of geometry defined by an entry radius R_i, exit radius R_o and converging angle α is also given by Equations A3.4-A3.6 (omitting the increment notation). Thus

Rewriting this equation yields

$$P_{ent} - P_s = \frac{\lambda \tan\alpha}{3}\left[\frac{4Q}{\pi R_o^3}\right]\left[1 - \left(\frac{R_o}{R_i}\right)^3\right] \qquad \text{(A3.7)}$$

$$\lambda = \frac{P_{ent} - P_s}{\frac{\tan\alpha}{3}\left[\frac{4Q}{\pi R_o^3}\right]\left[1 - \left(\frac{R_o}{R_i}\right)^3\right]} \qquad \text{(A3.8)}$$

Thus the extensional viscosity λ can be determined using Equation A3.8 where P_s is calculated using Equation A3.4 and P_{ent} is the experimentally measured entrance pressure drop.

The maximum average strain rate $\dot{\varepsilon}_{av}$ is related to the apparent shear-rate at the exit by

$$\dot{\varepsilon}_{av} = \frac{\tan\alpha}{2}\left(\frac{4Q}{\pi R_o^3}\right) \qquad \text{(A3.9)}$$

Equations A3.8 and A3.9 can be used to analyse entrance pressure drop versus flow rate data obtained using constricted (cone entry) converging flow geometries in terms of extensional viscosity and average strain rate value.

For freely converging flow the total pressure drop in an element ΔP_{ent} (Equation A3.6) was minimised with respect to the converging angle α of the element. The total pressure drop over the entire converging flow region was then given by the sum of the minimised pressure drops for all elements, taking the limit of this summation as the length of the individual elements tend to zero. The minimised total pressure drop P_{ent} for free convergence is given by the expression

$$P_{ent} = \frac{4\sqrt{2}}{3(n+1)} \left(\frac{4Q}{\pi R_o^3}\right) \left[\left(\eta_{ap} \times \lambda\right) \Big|_{r=R_o}\right]^{\frac{1}{2}} \qquad \text{(A3.10)}$$

The entry angle α_o formed by the flow at the die entrance is given by

$$\tan\alpha_o = \left[\left(\frac{2\eta_{ap}}{\lambda}\right) \Big|_{r=R_o}\right]^{1/2} \qquad \text{(A3.11)}$$

and the primary-secondary boundary profile by

$$h = \frac{\sqrt{2}\, r}{(3n-1)} \left[\left(\frac{r}{R_o}\right)^{\frac{3n-1}{2}} - 1\right] \left[\left(\frac{\lambda}{\eta_{ap}}\right) \Big|_{r=R_o}\right]^{\frac{1}{2}} \qquad \text{(A3.12)}$$

where h is the upstream distance from the die entry plane and r the radial position.

Rewriting Equation A3.10 yields the extensional viscosity λ

$$\lambda = \left[\frac{3(n+1)P_{ent}}{4\sqrt{2}\left(\frac{4Q}{\pi R_o^3}\right)}\right]^2 \frac{1}{\eta_{ap}\big|_{r=R_o}} \qquad \text{(A3.13)}$$

Thus given the apparent shear viscosity, Equations A3.1 and A3.3, the extensional viscosity λ can be determined using A3.13 where P_{ent} is the experimentally measured entrance pressure drop.

The average strain rate $\dot{\varepsilon}_{av}$ at the die entrance is given by

$$\dot{\varepsilon}_{av} = \left(\frac{2Q}{\pi R_o^3}\right) \left[\left(\frac{2\eta_{app}}{\lambda}\right) \Big|_{r=R_o}\right]^{\frac{1}{2}} \qquad \text{(A3.14)}$$

Equations A3.13 and A3.14 can be used to analyse entrance pressure drop versus flow rate data obtained using the flat entry geometry ($\alpha = 90^\circ$) in terms of extensional viscosity and strain rate.

In deriving this model it was assumed that the extensional viscosity was independent of strain rate. However, if the extensional viscosity of the fluid is calculated separately for each flow rate then an estimate of the strain rate dependence of extensional viscosity can be obtained.

Appendix A4: Gibson converging flow model

For reasons of consistency the notation used in this Appendix is not necessarily the same as that used in the original reference [10].

Gibson (10) developed a model for determining the extensional viscosity of fluids from constricted converging flow data only. However, he proposed that the model could be used for entrance pressure drop data obtained using contraction geometries with entry angle α of up to 90°. The author commented that although the secondary flow region had a significant effect on the appearance of the flow field in the entry region, it had only a small effect on the entrance pressure drop. Thus no distinction between constricted and free convergence data was made. The model cannot be used to predict the position of any free convergence primary-secondary flow boundary.

The converging flow model allows for both the shear and extensional viscosities to be described by independent power-law models:

$$\eta = \eta_o \dot{\gamma}^{n-1} \tag{A4.1}$$

$$\lambda = \lambda_o \dot{\varepsilon}^{m-1} \tag{A4.2}$$

where η_o and λ_o are functions of temperature, $\dot{\gamma}$ and $\dot{\varepsilon}$ are the shear rate and strain rate respectively and n and m are constants. The analysis of the converging flow region was carried out by dividing the region into two parts A and B, Figure A4.1. In region A the pressure drop contributions due to both the shear and extensional flow of the fluid were considered. In region B only the pressure drop contribution due to extensional flow was considered. The total pressure drop was calculated as being the sum of the shear component $P_{A,S}$ and the extensional components $P_{A,E}$ and $P_{B,E}$ where $_S$ and $_E$ indicate shear and extension and $_A$ and $_B$ indicate the regions A and B. These pressure drop components are given by Equations A4.3, A4.4 and A4.6 respectively. The shear flow pressure drop was calculated on the basis of a fully developed shear flow velocity profile transformed onto a spherical boundary coordinate system. The strain rate used was an average for the section, Equation A4.5, and was therefore independent of the assumed velocity profile. The three components of pressure drop in the contraction region are:

$$P_{A,S} = \frac{2\eta_o \left(\dot{\gamma}_{ap}^{n}\big|_{r=R_o}\right) \sin^{3n}\alpha}{3n\alpha^{(1+3n)}} \left(\frac{1+3n}{4n}\right)^{n} \left(1 - \left(\frac{R_o}{R_i}\right)^{3n}\right) \tag{A4.3}$$

$$P_{AE} = \frac{2\lambda_o}{3n} (\dot{\varepsilon}_1)^{m} \left(1 - \left(\frac{R_o}{R_i}\right)^{3m}\right) \tag{A4.4}$$

where the average strain rate $\dot{\varepsilon}_1$ is given by

$$\dot{\varepsilon}_1 = \left(\dot{\gamma}_{ap}\big|_{r=R_o}\right) \frac{\sin\alpha\ (1+\cos\alpha)}{4} \qquad \text{(A4.5)}$$

and

$$P_{B,E} = \frac{\lambda_o\left(\dot{\gamma}_{ap}\big|_{r=R_o}\right)}{4^m}\ \phi\ (m,\alpha) \qquad \text{(A4.6)}$$

where

$$\dot{\gamma}_{ap}\big|_{r=R_o} = \frac{4Q}{\pi R_o^3} \qquad \text{(A4.7)}$$

and

$$\Phi\ (m,\alpha) = \int_o^{\alpha} (1+\cos\beta)^{m-1}\ \sin^{m+1}\beta\, d\beta \qquad \text{(A4.8)}$$

$\Phi(m,\alpha)$ was solved by numerical iteration. The total entrance pressure drop P_{ent} is given, assuming additivity, as

$$P_{ent} = P_{A,S} + P_{A,E} + P_{B,E} \qquad \text{(A4.9)}$$

If this is rewritten in terms of the pressure drop due to extensional flow in regions A and B, then

$$P_{ent} - P_{A,S} = P_{A,E} + P_{B,E} \qquad \text{(A4.10)}$$

Thus, substituting for $P_{A,E}$ and $P_{B,E}$ using Equations A4.4 and A4.6,

$$P_{ent} - P_{A,S} = \lambda_o\left(\dot{\gamma}_{ap}^{m}\big|_{r=R_o}\right)\left[\left(\frac{2}{3m}\right)\left(\frac{\sin\alpha\ (1+\cos\alpha)}{4}\right)^m\left(1 - \left(\frac{R_o}{R_i}\right)^{3m}\right) + \phi\ (m,\alpha)/4^m\right] \qquad \text{(A4.11)}$$

P_{ent} is the experimentally measured entrance pressure drop and $P_{A,S}$ is calculated using Equation A4.3. A plot of log $(P_{ent} - P_{A,S})$ versus log $(\dot{\gamma}_{ap}|_{r=Ro})$ has a gradient that is equal to

the extensional viscosity power-law exponent m and intercept value $\log(P_{int}')$ where P_{int}' is given by

$$P_{int}' = \lambda_o \left[\left(\frac{2}{3m} \right) \left(\frac{\sin\alpha \ (1+\cos\alpha)}{4} \right)^m \left(1 - \left(\frac{R_o}{R_i} \right)^{3m} \right) + \frac{\phi \ (m,\alpha)}{4^m} \right] \qquad \text{(A4.12)}$$

Rewriting A4.12 yield the extensional viscosity pre-exponent λ_o thus

$$\lambda_o = \frac{P_{int}'}{\left[\left(\frac{2}{3m} \right) \left(\frac{\sin\alpha \ (1+\cos\alpha)}{4} \right)^m \left(1 - \left(\frac{R_o}{R_i} \right)^{3m} \right) + \frac{\phi \ (m,\alpha)}{4^m} \right]} \qquad \text{(A4.13)}$$

Thus Equations A4.13 and the gradient of the plot of log (P_{ent} - $P_{A,S}$) versus log ($\dot{\gamma}_{ap}|_{r=Ro}$) can be used to determine the extensional viscosity pre-exponent and exponent values.

Given the extensional viscosity exponent value m then individual extensional viscosity values can be determined by manipulation of Equations A4.2, A4.5 and A4.11 thus

$$\lambda = \frac{\left(P_{ent} - P_{A,S} \right) \dot{\varepsilon}_1^{m-1}}{\left(\dot{\gamma}_{ap} \right)^m \left[\left(\frac{2}{3m} \right) \left(\frac{\sin\alpha \ (1+\cos\alpha)}{4} \right)^m \left(1 - \left(\frac{R_o}{R_i} \right)^{3m} \right) + \frac{\phi \ (m,\alpha)}{4^m} \right]} \qquad \text{(A4.14)}$$

where $\dot{\varepsilon}_1$ is given by Equation A4.5.

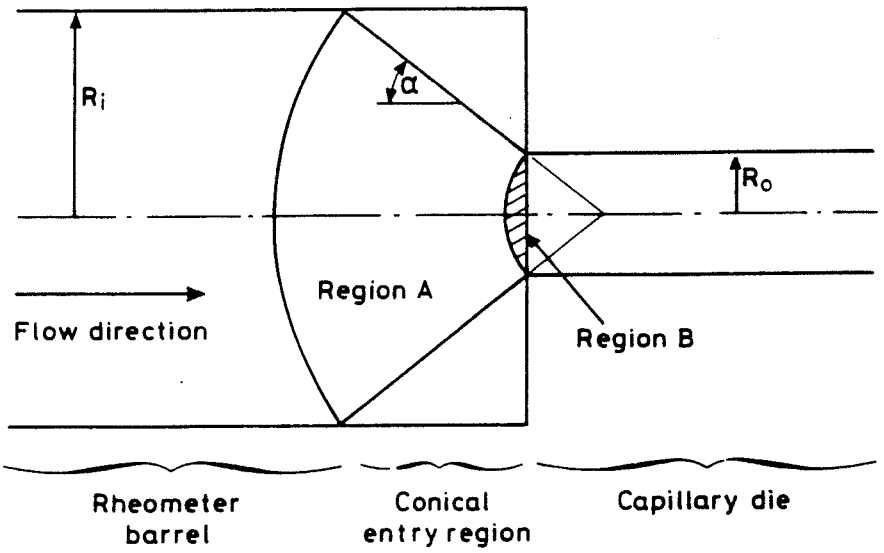

Figure A4.1 Entry geometry definition for the Gibson model (10).

Appendix A5: Binding viscous converging flow model

For reasons of consistency the notation used in this Appendix is not necessarily the same as that used in the original reference [8].

The approach used by Binding [8] was to consider the minimisation of the rate of change of energy occurring in the converging flow of a fluid. This change in energy results from the process of viscous dissipation and also from a change in kinetic energy of the fluid. The model applies to free convergence flow only. Independent power-law models identical to those used by Gibson [10] were used to describe the shear and extensional viscosities, Equations A4.1 and A4.2. A fully developed power-law shear flow velocity profile was assumed. Local shear and extensional deformation rates $\dot{\gamma}$ and $\dot{\varepsilon}$ were derived using this velocity profile and are given by

$$\dot{\varepsilon} = \left(\frac{3n+1}{n+1}\right) \frac{Q}{\pi R^3} \left(\left(\frac{3n+1}{n}\right) \left(\frac{r}{R}\right)^{1+1/n} - 2 \right) \frac{dR}{dz} \qquad \text{(A5.1)}$$

and

$$\dot{\gamma} = - \left(\frac{3n+1}{n}\right) \frac{Q}{\pi R^3} \left(\frac{r}{R}\right)^{1/n} \qquad \text{(A5.2)}$$

where z and r are defined by a cylindrical coordinate system, Figure A5.1, and R defines the primary-secondary flow boundary (dR/dZ is negative in value). It was noted that $\dot{\varepsilon}$ is positive at r = 0, and negative at r = R. The calculated negative strain rates in the converging flow model arise as a consequence of the assumed velocity profile.

Expressions for the shear and extensional viscous dissipation in a conical element of the converging flow field were derived using Equations A5.1 and A5.2. The expression for the rate of change of kinetic energy of the fluid, Equation A5.5, was also derived from consideration of the velocity field. However, this contribution is considered to be minimal for polymer melts and can be ignored. Thus the rate of change of energy of the fluid flowing in the converging section was determined as the sum of the rates of shear and extensional viscous dissipation, this being obtained by integration of the dissipation terms over the flow volume. This was then minimised with respect to the shape of the primary-secondary flow boundary to yield the flow field relating to minimum energy dissipation. The entrance pressure drop P_{ent} in the converging section was related to the rate of change of energy of the system $\dot{E}$ by

$$P_{ent} = \frac{\dot{E}}{Q} \qquad \text{(A5.3)}$$

By substituting for the minimised rate of change of energy $\dot{E}$ the entrance pressure drop was given by

$$P_{ent} = \frac{2\eta_o (1+m)^2}{3m^2 (1+n)^2}\left(\frac{\lambda_o m(3n+1)n^m I_{nm}}{\eta_o'}\right)^{1/(1+m)} \dot{\gamma}_o^{m(n+1)/(1+m)}$$

$$x\left(1 - \beta^{3m(1+n)/(1+m)}\right) + \frac{K\dot{E}}{Q} \qquad \text{(A5.4)}$$

where the rate of change of kinetic energy $K\dot{E}$ is given by

$$K\dot{E} = \frac{3\rho Q^3 (3n+1)^2 (1-\beta^4)}{2(2n+1)(5n+3)\pi^2 R_o^4} \qquad \text{(A5.5)}$$

where ρ is the fluid density. Also

$$\dot{\gamma}_o = \left(\frac{3n+1}{4n}\right)\left(\frac{4Q}{\pi R_o^3}\right) \qquad \text{(A5.6)}$$

$$I_{nm} = \int_o^1 \left[\text{abs}\left(2 - \left(\frac{3n+1}{n}\right)\varphi^{1+1/n}\right)\right]^{m+1} \varphi \, d\varphi \, . \qquad \text{(A5.7)}$$

and

$$\beta = \left(\frac{R_o}{R_i}\right) \qquad \text{(A5.8)}$$

where R_o is the die radius and R_i is the barrel radius. The optimised primary-secondary flow boundary relating to minimum energy dissipation was defined by

$$\frac{dR}{dz} = -(n+1)\left(\frac{k}{\ell m(3n+1)n^n I_{nm}}\right)^{1/(m+1)}\left(\frac{(3n+1)Q}{\pi R^3}\right)^{\frac{n-m}{m+1}} \qquad \text{(A5.9)}$$

where the attachment length L_v of the vortex to the barrel wall is given by

$$L_v = \frac{(1+m)}{2(n+1)(2m-3n-1)}\left(\frac{\lambda_o (3n+1) m\, n^m I_{nm}}{\eta_o'}\right)^{1/(1+m)} \qquad \text{(A5.10)}$$

$$x\, \dot{\gamma}_o^{(m-n)/(1+m)}\, x\left(1 - \beta^{(2m-3n-1)/(1+m)}\right) x\, \beta \qquad \text{(A5.11)}$$

From Equations A5.1 and A5.9 the strain rate everywhere in the converging flow region can be determined.

Assuming that the contribution due to the kinetic energy term in Equation A5.4 is negligible then the gradient s^* of a plot of log (P_{ent}) versus log ($\dot{\gamma}_o$) is given, using Equation A5.4, as

$$s^* = m(n+1)/(1+m) \qquad \text{(A5.12)}$$

By rearranging A5.12 the extensional viscosity power-law exponent m is given by

$$m = \frac{s^*}{n+1-s^*} \qquad \text{(A5.13)}$$

Thus, given the value of the shear viscosity exponent n, m can be determined. The integral I_{nm}, Equation A5.7, can then be evaluated numerically. Assuming that the contribution due to the kinetic energy term in Equation A5.4 is negligible then the value of the intercept log(P_{int}^*) of the log (P_{ent}) axis of the plot of log (P_{ent}) versus log ($\dot{\gamma}_o$) is given, using Equation A5.4, as

$$P_{int}^* = \frac{2\eta_o(1+m)^2}{3m^2(1+n)^2}\left(\frac{\lambda_o\, m(3n+1)\, n^m\, I_{nm}}{\eta_o'}\right)^{1/(1+m)}\left(1-\beta^{3m(1+n)/(1+m)}\right) \qquad \text{(A5.14)}$$

Thus λ_o is given by

$$\lambda_o = \frac{\eta_o'}{m(3n+1)n^m I_{nm}}\left[\frac{P_{int}^*}{\left(\frac{2\eta_o(1+m)^2}{3m^2(1+n)^2}\right)\left(1-\beta^{(3m(1+n)/(1+m))}\right)}\right]^{1+m} \qquad \text{(A5.15)}$$

The maximum strain rate occurring in the flow is given, using Equations A5.1 and A5.9, as

$$\left|\dot{\varepsilon}\right|_{max} = (n+1)\left(\frac{\eta}{\lambda_o m(3n+1)n^m I_{nm}}\right)^{1/(1+m)}\dot{\gamma}_o^{(1+n)/(1+m)} \qquad \text{(A5.16)}$$

and the centre-line strain rate by

$$\left|\dot{\varepsilon}\right|_{cl} = 2\left(\frac{\eta_o\, n}{\lambda_o m(3n+1)I_{nm}}\right)^{1/(1+m)}\dot{\gamma}_o^{(1+n)/(1+m)} \qquad \text{(A5.17)}$$

Thus the extensional power-law parameters m and λ_o can be deduced using Equations A5.13 and A5.15 respectively, and the shear rates that characterise the flow by either Equations A5.16 or A5.17.

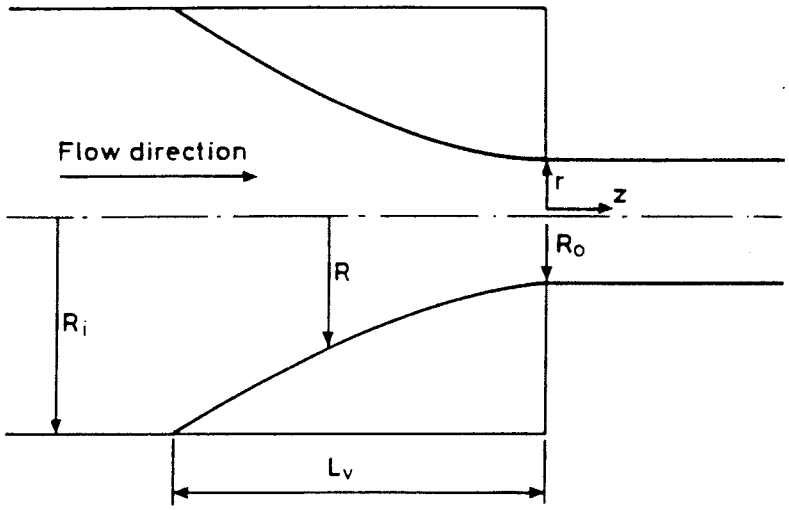

Figure A5.1 Entry geometry definition for the Binding model (8).

Appendix A6: Binding viscoelastic converging flow model

For reasons of consistency the notation used in this Appendix is not necessarily the same as that used in the original reference [9].

The binding viscoelastic model was developed using the same principles as that of the viscous model, Appendix 5, but includes a dissipation term for viscoelasticity, the data for which are based on shear flow measurements of the first normal stress difference N_1.

The Couette correction, C, is defined by

$$C = P_{ent} \; / \left(2\tau_w\right) \tag{A6.1}$$

where τ_w is the wall shear stress in the die (see Section 6.2). The shear viscosity, extensional viscosity and first normal stress difference are given by the expressions

$$\eta = \eta_o \dot{\gamma}^{n-1} \tag{A6.2}$$

$$\lambda = \lambda_o \dot{\varepsilon}^{m-1} \tag{A6.3}$$

and

$$N_1 = N_{1,o} \dot{\gamma}^{p+1} \tag{A6.4}$$

A rate term A is defined such that

$$A = Q/\pi R_o^3 \tag{A6.5}$$

where R_o is the radius of the capillary die.

Solving an energy balance, following the method used for the purely viscous model, yields

$$C = \beta_1 A^{(m-n)/(1+m)} - \beta_2 A^{p+1-n} \tag{A6.6}$$

where

$$\beta_1 = \frac{(1+m)^2}{3m^2(1+n)^2}\left\{\frac{\lambda_o m(3n+1)^{1+m-n} n^n I_{nm}}{\eta_o}\right\}^{1/(m+1)} \qquad \text{(A6.7)}$$

and

$$\beta_2 = N_{1,o}(3n-1)(3n+1)\{(3n+1)/n\}^{p+1-n} / \{3\eta_o(2n+p+1)(3n+p+2)\} \qquad \text{(A6.8)}$$

The integral I_{nm} is given by

$$I_{nm} = \int_0^1 \left[abs\left\{2 - \left(\frac{3n+1}{n}\right)\phi^{(n+1)/n}\right\}\right]^{m+1} \phi d\phi \qquad \text{(A6.9)}$$

Note: there is an error in the original paper [9] relating to the power to which ϕ is raised in the integral: it should be (n+1)/n as stated above rather than n+1/n as in [9].

Rewriting A6.6 gives

$$\beta_1 A^{(m-n)/(1+m)} = C - \beta_2 A^{p+1-n} \qquad \text{(A6.10)}$$

Given the values of the parameters for the shear viscosity and first normal stress difference power-law models the term β_2 can be calculated. C is calculated using Equation A6.1 and the wall shear stress, determined from shear viscosity and shear rate. Thus the value of the right hand side of this equation can be evaluated.

Plot the logarithm of the values of the left hand side of this expression as a function of log (A). The intercept of this plot with the y-axis (i.e. at A = 1) is equal to $\log(\beta_1)$ thus yielding the value of β_1. The gradient of this plot s' is given, using Equation A6.10, by the expression

$$s' = \frac{m-n}{1+m} \qquad \text{(A6.11)}$$

Thus, given the value of the shear rate exponent n, the value of m can be deduced.

$$m = \frac{s'+n}{1-s'} \qquad \text{(A6.12)}$$

The value of the integral I_{nm}, Equation A6.9, can now be evaluated.

Finally, Equation A6.7 can be rewritten to yield the extensional viscosity pre-exponent λ_o as

$$\lambda_o = \frac{\eta_o\left(\beta_1\left(\frac{3m^2(1+n)^2}{(1+m)^2}\right)\right)^{1+m}}{m(3n+1)^{1+m-n}n^n I_{nm}} \qquad \text{(A6.13)}$$

Thus λ_o can be determined as all values on the right hand side are now known.

The strain rates characterising this flow are the same as that of the Binding viscous model as the assumptions made in defining the velocity field were the same. The maximum strain rate occurring in the flow is given, using Equations A5.1 and A5.9, by

$$\left|\dot{\varepsilon}\right|_{\max} = (\mathrm{n}+1)\left(\frac{\eta}{\lambda_o m(3n+1)n^m I_{nm}}\right)^{1/(1+m)} \dot{\gamma}_o^{(1+n)/(1+m)} \qquad \text{(A6.14)}$$

and the centre-line strain rate by

$$\left|\dot{\varepsilon}\right|_{cl} = 2\left(\frac{\eta_o\, n}{\lambda_o m(3n+1)I_{nm}}\right)^{1/(1+m)} \dot{\gamma}_o^{(1+n)/(1+m)} \qquad \text{(A6.15)}$$

Appendix A7: Rides converging flow model

The formulation of the model is based on the principles used by Cogswell [7] except that a power-law is used to describe the extensional viscosity behaviour.

In the converging flow model it was assumed that shear viscosity η was described by the power-law behaviour

$$\eta = \eta_o \dot{\gamma}^{n-1} \tag{A7.1}$$

and extensional viscosity λ was described also by a power-law behaviour

$$\lambda = \lambda_o \dot{\varepsilon}^{m-1} \tag{A7.2}$$

where η_o and λ_o are constant for a given temperature, $\dot{\gamma}$ and $\dot{\varepsilon}$ are the shear rate and strain rate respectively and n and m are constants. The analysis considered that the converging flow region was comprised of a series of short truncated conical elements of decreasing diameter. The velocity profile of the flow in each element was assumed to be the same as that for fully developed shear flow. The shear flow pressure drop for the element was determined by integration over the length of the tapered element. The extensional flow pressure drop was based on the average extension rate over the length of the element, and as such was independent of the assumed velocity profile. The shear flow pressure drop ΔP_S and the extensional flow pressure drop ΔP_E for a conical element of entry radius R_i, exit radius R_o ($R_o < R_i$) and converging angle α are given by

$$\Delta P_s = 2 \frac{\left(\eta_{ap}\big|_{r=Ro}\right)}{3n \tan\alpha} \left[\frac{4Q}{\pi R_o^3}\right] \left[1 - \left(\frac{R_o}{R_i}\right)^{3n}\right] \tag{A7.3}$$

and

$$\Delta P_E = \frac{2\lambda_o (\tan\alpha)^m}{3m} \left[\frac{2Q}{\pi R_o^3}\right]^m \left[1 - \left(\frac{R_o}{R_i}\right)^{3m}\right] \tag{A7.4}$$

where $\eta_{ap}|_{r=Ro}$ denotes the apparent shear viscosity evaluated for the apparent shear-rate for flow rate Q in a channel of radius R_o. The total pressure drop ΔP_{ent} for the element was calculated, assuming additivity, as the sum of the shear and extensional flow pressure drops.

Thus

$$\Delta P_{ent} = \Delta P_s + \Delta P_E \qquad \text{(A7.5)}$$

For freely converging flow the total pressure drop in an element ΔP_{ent} (Equation A7.5) was minimised with respect to the converging angle α of the element. The total pressure drop over the entire converging flow region was then given by the sum of the minimised pressure drops for all elements, taking the limit of this summation as the length of the individual elements tend to zero. The minimised total pressure drop P_{ent} for free convergence is given by the expression

$$P_{ent} = \left(\frac{2\eta_o}{3n}\right)^{m/(1+m)}\left(\frac{2\lambda_o}{3m}\right)^{1/(1+m)}\left(\frac{n^{m/(1+m)}m^{1/(1+m)}}{\frac{m(1+n)}{1+m}}\right)\left(m^{1/(1+m)}+m^{-m/(1+m)}\right)\left[\left(\frac{3n+1}{4n}\right)\left(\frac{4}{\pi R_o^3}\right)\right]^{nm/(1+m)}\times$$

$$\times\left(\frac{2}{\pi R_o^{\,3}}\right)^{m/(1+m)} \times Q^{nm/(1+m)}Q^{m/(1+m)} \qquad \text{(A7.6)}$$

A plot of log (P_{ent}) versus log (Q) has a gradient s'' and an intercept value of log (P_{int}'') where

$$s'' = \frac{m(1+n)}{1+m} \qquad \text{(A7.7)}$$

Thus the extensional viscosity exponent m is given by

$$m = \frac{s''}{1+n-s''} \qquad \text{(A7.8)}$$

Using the intercept value P_{int}'', Equation A7.6 can be rewritten to yield

$$\lambda_o = \frac{3m}{2}\left(\frac{P_{int}''}{\left(\frac{2\eta_o}{3n}\right)^{\frac{m}{1+m}}\left(\frac{n^{m/(1+m)}m^{1/(1+m)}}{\frac{m(1+n)}{1+m}}\right)\left(m^{1/(1+m)}+m^{-m/(1+m)}\right)\left[\left(\frac{3n+1}{4n}\right)\left(\frac{4}{\pi R_o^3}\right)\right]^{\frac{nm}{1+m}}\left(\frac{2}{\pi R_o^{\,3}}\right)^{\frac{m}{1+m}}}\right)^{1+m} \qquad \text{(A7.9)}$$

Thus λ_o can be determined.

The entry angle α_o formed by the flow at the die entrance is given by

$$\tan\alpha_o = \left(\frac{2^m \eta_{ap} \dot{\gamma}^{1-m}}{m\lambda_o}\right)^{1/(1+m)} \qquad \text{(A7.10)}$$

The average strain rate $\dot{\varepsilon}_{av}$ at the die entrance is given by

$$\dot{\varepsilon}_{av} = \frac{\dot{\gamma}_{ap}}{2}\left(\frac{2^m \eta_o}{m\lambda_o}\left(\frac{3n+1}{4n}\right)^n \dot{\gamma}_{ap}^{(n-m)}\right)^{1/(1+m)} \qquad \text{(A7.11)}$$

These expressions simplify in the case of m = 1 to the equivalent expressions for the Cogswell model [7].

Given the value of the extensional viscosity exponent m then individual extensional viscosity values can be determined, using Equations A7.2 and A7.6, as

$$\lambda = \frac{3m}{2}\left(\dot{\varepsilon}_{av}\right)^{m-1}\left(\frac{P_{ent}}{\left(\frac{2\eta_o}{3n}\right)^{\frac{m}{1+m}}\left(\frac{n^{m/(1+m)}m^{1/(1+m)}}{\frac{m(1+n)}{1+m}}\right)\left(m^{1/(1+m)}+m^{-m/(1+m)}\right)\left[\left(\frac{3n+1}{4n}\right)\left(\frac{4Q}{\pi R_o^3}\right)\right]^{\frac{nm}{1+m}}\left(\frac{2Q}{\pi R_o^{\,3}}\right)^{\frac{m}{1+m}}}\right)^{1+m} \qquad \text{(A7.12)}$$

ENERGY